

## Technical Articles

- Design of Gas Stripping Module for Identification of Dry Rupture in Fast Breeder Reactors
- Vertical Graphene Nanosheets: An Emerging Material for Energy Storage

## Young Officer's Forum

- Low Cycle Fatigue-High Cycle Fatigue Interaction in Type 316LN Stainless Steel

## Young Researcher's Forum

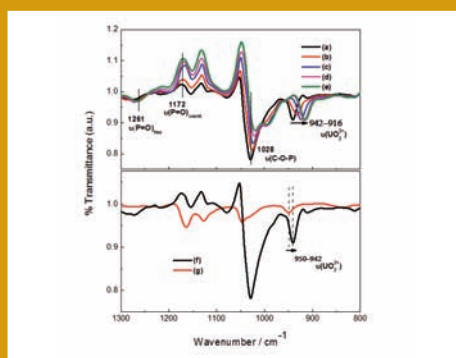
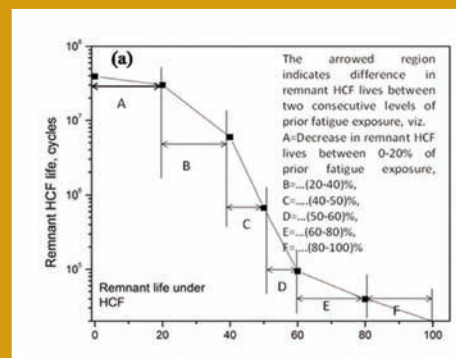
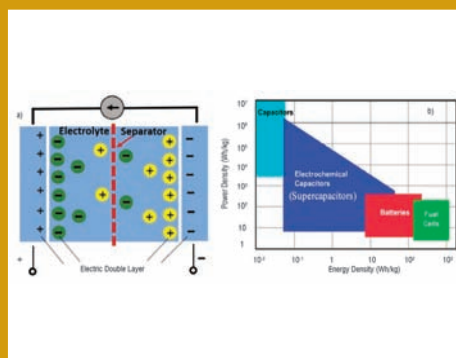
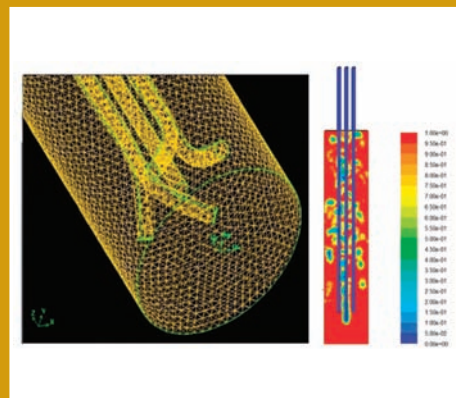
- Spectroscopic Investigations on the Coordination Environment of Uranyl Ion in Ionic Liquid Medium

## Conference and Meeting Highlights

- IGCAR - CEA Meeting in Nuclear Technology  
14<sup>th</sup> Annual Meeting on LMFBR Safety  
Technical Annual Meeting for JHR Collaboration
- 26<sup>th</sup> Prof. Brahm Prakash Memorial Materials Quiz Grand Finale (BPMMQ 2018)
- National Conference URJAVARAN – 2018
- Indo-UK Civil Nuclear Collaboration Review Meeting
- Report on Radiation Awareness Program at Kalpakkam
- Second Quadrennial International CONFERENCE on Structural Integrity (ICONS2018)

## HBNI-IGCAR Corner

## Awards & Honours



## *From the Editorial Committee*

### *Dear Reader*

We take this opportunity to wish you all a very Happy New Year, 2019.

It is our pleasant privilege to forward a copy of the latest issue of IGC Newsletter (Volume 119, January 2019 issue).

In the first technical article Ms. R. Vijayashree and colleagues from Reactor Design Group have discussed about the “Design of Gas stripping module for identification of dry rupture in Fast Breeder Reactors”.

In the second technical article Dr. S. R. Polaki and colleagues from Materials Science Group have discussed about the “Vertical Graphene Nanosheets: An Emerging Material for Energy Storage”.

This issue’s Young Officer’s Forum features an article by Dr. Aritra Sarkar, from Metallurgy and Materials Group discussing about the Low Cycle Fatigue-High Cycle Fatigue Interaction in Type 316LN Stainless Steel.

Shri G. Murali Krishna has described about Spectroscopic Investigations on the Coordination Environment of Uranyl Ion in Ionic Liquid Medium in the Young Researcher’s Forum.

We are happy to share with you the awards, honours and distinctions earned by our colleagues.

We look forward to your comments, continued guidance and support.

With best wishes and personal regards

Editorial Committee, IGC Newsletter

## New Year Message

### Dear Colleagues,

I wish all of you and your families a very successful, healthy and prosperous New Year 2019.

In the year gone by, our FBTR operated at a power level of 32 MWt for the first time in its history in the 27<sup>th</sup> irradiation campaign, delivering to the grid electrical output of 7 MWe. As part of in-service inspection, the internals of FBTR reactor vessel of the reactor were satisfactorily inspected. The U-233 based 30 kWt KAMINI reactor, relicensed till June 2020, continued to operate for neutron radiography of pyro-devices, cords and cartridges from ISRO for their future missions, neutron activation analysis, neutron detector testing etc. More collaboration with academic institutions and industries are underway for utilising the capabilities offered by KAMINI reactor. For the commissioning of 500 MWe Prototype Fast Breeder Reactor, IGCAR continues to provide all necessary technical and manpower support.

Preliminary conceptual design document of FBTR-2, a 100 MWt loop-type metal-fuel test reactor, has also been prepared. The Metal Fuel Pin Fabrication Facility was dedicated to the nation by Honourable President of India on 15<sup>th</sup> May 2018, and sodium bonded metal fuel pins fabricated in this facility is under test-irradiation in FBTR. To establish viability of aqueous reprocessing of metal fuel, as an alternate to pyro-chemical reprocessing, dissolution aspects of metal-alloy fuels have been studied.

Facilities for irradiation capsule fabrication, spark-plasma sintering of B<sub>4</sub>C pellets, remote impact testing of irradiated structural materials and mobile sodium purification loop in FBTR flooding circuit have been commissioned. Further, an advanced phased array ultrasonic based methodology for in-service inspection of thick dissimilar-metal weld for FBRs as also DISHA, a weld inspection device for periodic remote visual examination and ultrasonic testing of dissimilar-metal weld between roof-slab and main vessel of PFBR, have been



successfully developed. Other noteworthy developments include composition-optimized metal waste form for pyro-chemical reprocessing application, special dissimilar metal welding technique and weld inspection methodology for turbine rotor of advanced ultra-supercritical coal-fired thermal power plants, virtual control panel to study Human Machine Interface, indigenous design of CPU boards, IT-enabled Knowledge Management System and deployment of wireless sensor networks for various applications. A state-of-the-art facility for calibration of gamma-radiation survey instruments of radiological facilities has been commissioned and accredited by AERB in April 2018.

With the renewal of operating license of CORAL for the next 5 years, routine reprocessing campaigns of FBTR fuel have commenced. Towards commissioning of DFRP, water runs have been completed, leak testing of containment systems is in progress and inactive chemical runs are scheduled. Construction activities at FRFCF continue to make steady progress, with a notable achievement being that of a single largest pour in DAE comprising an uninterrupted 94-hour 7200 cu.m. concrete pour.

Twenty nine scientists and engineers (OCES-2017, 12<sup>th</sup> Batch) successfully completed their orientation programme at BARC

Training School at IGCAR and were placed in various units of DAE, and the different programmes of HBNI continued to make desired progress. The performance of the students in board examinations from the 2 KVs and 3 AECSs has been exemplary.

The year ahead too has a number of challenges, with the foremost being the technical support towards commissioning of PFBR, refurbishment of FBTR and KAMINI for continued uninterrupted operation, finalisation of preliminary design of future FBRs, development of pre-service and in-service inspection system for FBRs, developing repair technology of steam generator tubes, commissioning and operating DFRP for regular reprocessing of FBTR fuel, development of improved imaging and inspection techniques for advanced NDE and enhancement of radiological safety. IGCAR would also be appropriately celebrating the International Year of the Periodic Table 2019, declared by UNESCO to mark 150 years since Dimitry Mendeleev proposed the idea of the periodic table.

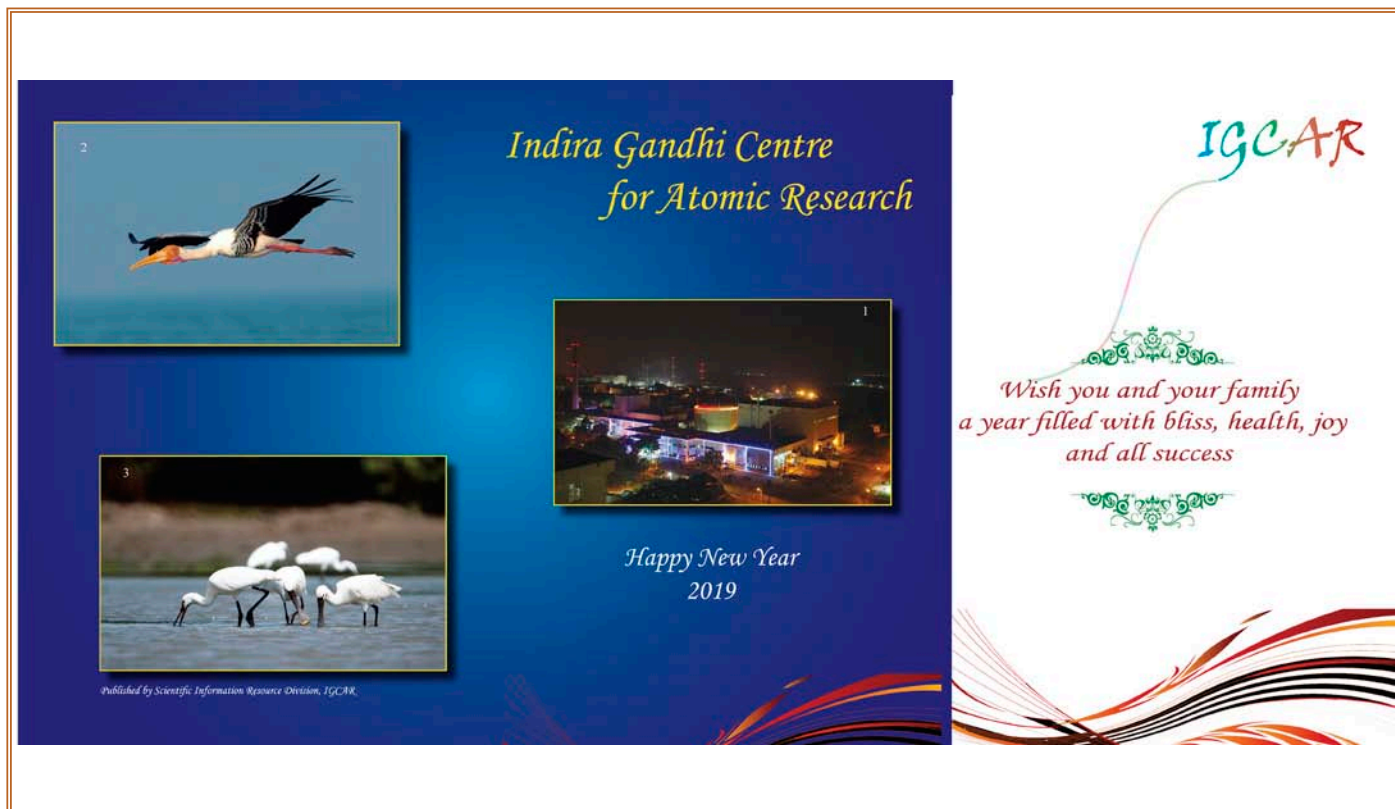
GSO continued to construct and efficiently maintain the residential and infrastructural buildings and enhancing the medical facilities

in the twin townships of Kalpakkam and Anupuram. In fact, the serene, green and clean was recognized as the second cleanest among all the DAE townships. The medical group continued to improve the quality of health care to the CHSS beneficiaries, including setting up an outsourced pharmacy and establishing the CHSS facility at IMSc Chennai.

The Administration and Accounts departments of IGCAR and GSO continued to provide commendable services support, guiding and ensuring the timely execution of the programmes.

These achievements in IGCAR, GSO and AECS would not have been possible without the dedicated efforts of all our colleagues, and we look forward to more vigorous efforts in this year as well.

(Dr. Arun Kumar Bhaduri)



## Design of Gas Stripping Module for Identification of Dry Rupture in Fast Breeder Reactors

The burnup achieved in a fast reactor fuel pin is much higher than that in a thermal reactor. As a result of this, the quantity of fission products and the fission gas pressure in fast reactor fuel pins are also high. Also, the fast reactor fuel pins operate at elevated temperatures well in the creep regime and are subjected to large irradiation dose. The fuel subassembly of a prototype fast breeder reactor contains 217 fuel pins, arranged in a triangular pitch and housed inside a hexagonal wrapper. Clad tube acts as primary boundary between fuel and coolant. The fission products are confined within the clad. Fuel pins have a life span of ~2 reactor years. Clad tube failure can happen in the initial stages due to minor manufacturing defects and at later stage due to irradiation, creep and thermal cycling effects, pressure build-up due to fission gas etc. Fuel pin failures are classified as dry rupture and wet rupture.

During wet rupture, sodium enters the fuel pin and interacts with fissile fuel. Fission products as well as fuel particles containing delayed neutron precursors will get released into sodium pool during wet rupture. The localization of fuel subassembly with failed fuel pin is carried out using Failed Fuel Location Module (FFLM) by Delayed Neutron Detection (DND) method. FFLM is deployed after getting indication of fuel pin failure from Cover Gas Monitoring System and global DND detectors held near IHX.

A dry rupture event is accompanied by release of gaseous fission products viz., isotopes of xenon and krypton into sodium without fuel-coolant interaction. These gases diffuse into cover gas and increase activity of Reactor Containment Building (RCB) depending on the leak rate of cover gas to RCB. Once a dry rupture is detected, the reactor operation is continued till the dry rupture gets converted into wet rupture and then failed fuel localisation will be carried out.

Dry rupture may prevail in reactor over weeks or month until it converts into wet rupture. Localisation of failed fuel subassembly at dry rupture stage is taken as R&D activity so that it can be replaced with a fresh subassembly at earliest.

The gaseous fission products, xenon and krypton emit gamma rays and hence dry rupture can be detected by monitoring the presence of these radioactive gases in sodium sampled from fuel subassembly. FFLM is equipped with a selector valve and DC conduction pump to selectively pump sodium from each fuel subassembly and send to a capacity for localizing failed fuel pin with wet rupture by DN detection. A schematic sketch of FFLM is shown in Figure 1. The sampled sodium will have high gamma activity due to the presence of <sup>24</sup>Na. Due to this high back ground

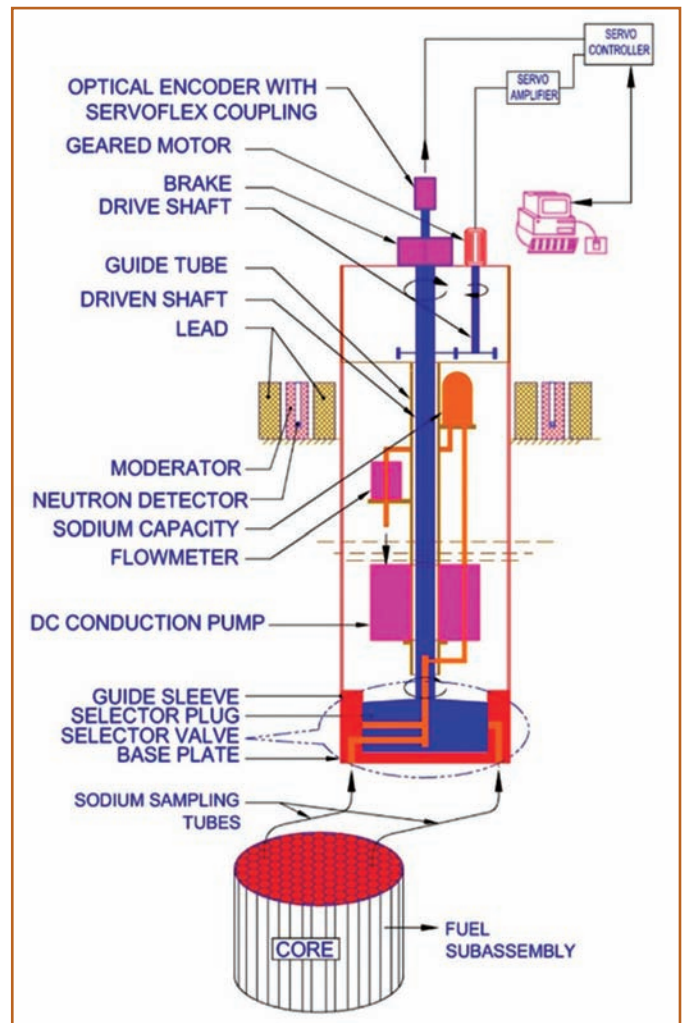


Figure 1: Schematic of FFLM

activity, detection of gamma emitted by gaseous fission products released during dry rupture is impossible. Hence there is a need to separate the fission gases from sodium sample for gamma monitoring.

A gas stripping module is designed to separate gaseous fission products from sampled sodium. Solubility of xenon and krypton is less in sodium ( $2.87 \times 10^{-9}$  mole per mole Na at 550°C) and hence most of the gases will remain in the form of small bubbles in the sample. These fission gases can be trapped by continuous purging of argon into sampled sodium. Xenon and krypton will mix into argon when they come in contact with each other during purging. The diffusivity of xenon and krypton in argon is ~1000 times more than that in sodium. The sampled gas after purging will be sent to the detector, located away from active sodium for detecting the presence of fission gases by gamma monitoring.

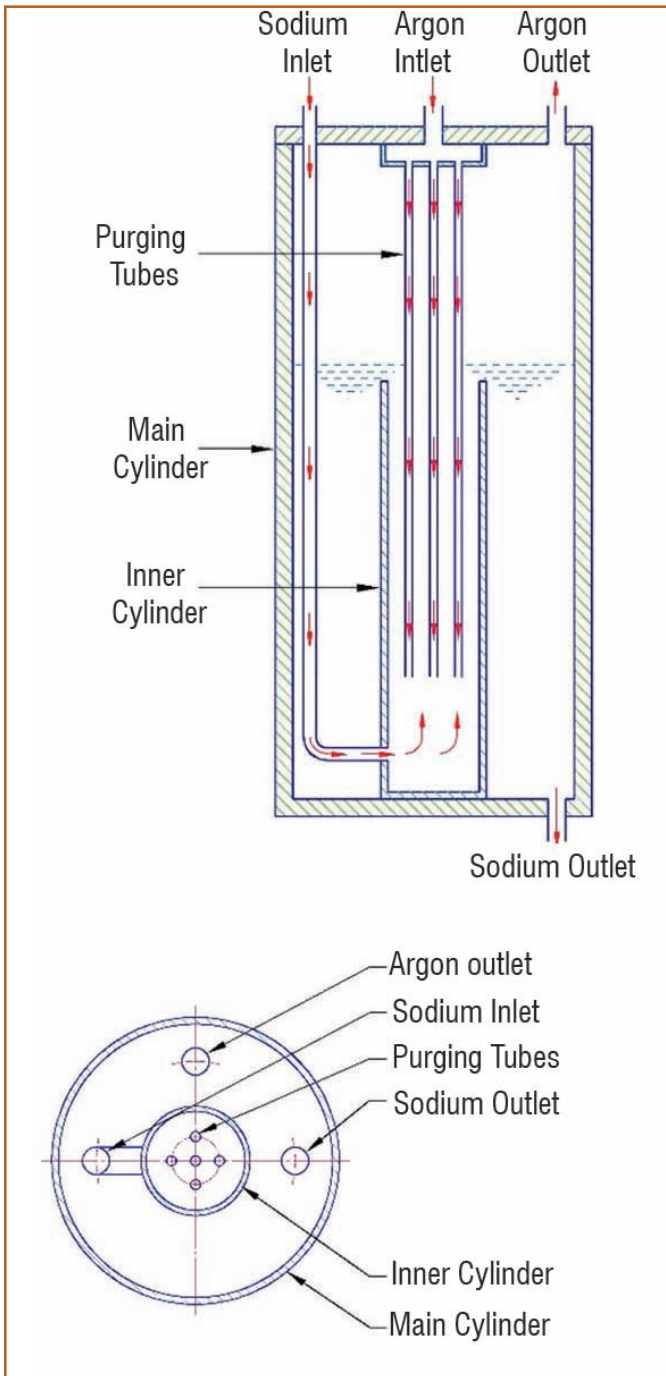


Figure 2: Gas stripping module

A gas stripping module to be retrofitted in FFLM has been designed and is shown in Figure 2. It consists of two concentric cylinders. Sampled sodium enters into inner cylinder, from its bottom end. After filling the inner cylinder, sodium overflows and enters the main cylinder. A small opening is provided at the bottom of main cylinder through which sodium returns back to existing sodium line. Fresh Argon for stripping is supplied to a header, provided at the top and distributed in the inner cylinder through small tubes. This arrangement is designed to provide maximum possible retention time for sodium in the capacity to increase

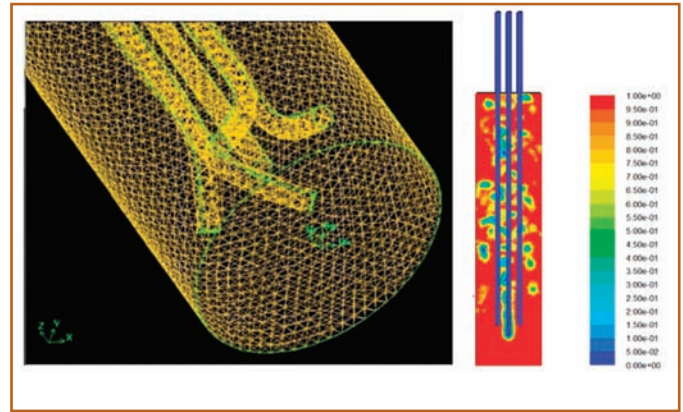


Figure 3: Argon gas distribution in inner cylinder

the probability of interaction of stripping gas with fission gas bubbles. The purged gas along with fission gases gets collected in the space above sodium free level. Gas samples will be taken from this space and supplied to gamma detectors through a tube connected to the top end of the capacity. This module can be attached in the return line of sampled sodium in FFLM without affecting its function of detecting wet rupture.

Hydraulic study of sodium and argon flow was carried out. The presence of module in the sampling line will add an additional pressure drop of 5.5 kPa which can be supplied by the present DC conduction pump.

The mass transfer efficiency of this module depends on contact area of gases and time. The design flow rate of sodium in the sampling line of FFLM is 100 cc/s which is fixed based on wet rupture detection consideration. The volume of module is fixed based on space constraints in FFLM. Hence to increase the probability of interaction of argon stripper gas and fission gas bubbles, various options were studied such as providing perforated purging tubes, providing bend at the bottom end of tubes, providing perforated header at the bottom of inner cylinder etc. Hydraulic analysis was carried out to study the efficiency for each of these cases.

It is found that providing bends at the bottom end of tubes gives better distribution of gases thereby increasing the probability of bubbles to get into contact with each other. The model used for hydraulic analysis and the result for the selected case is shown in Figure 3.

Conceptual design of gas stripper for localizing fuel pin with dry rupture is completed. Experiments are planned in sodium to find out the stripping efficiency. Further hydraulic characteristics will be established by water testing. The system will be qualified in sodium before implementing the same in the reactor.

*R. Vijayashree and colleagues  
Reactor Design Group*

## Vertical Graphene Nanosheets: An Emerging Material for Energy Storage

Energy storage devices garnered a lot of attention in the recent past, due to ever rising usage of electronic gadgets by technology driven modern society. Additionally, since industrial revolution, consumption of fossil fuel has been growing tremendously leading to massive CO<sub>2</sub> emissions, which causes global warming, a big threat to the environment. Development of renewable energy sources (solar, wind, tidal and bio fuels) is the plausible alternate to minimize the consumption of fossil fuels and to curtail CO<sub>2</sub> emissions. Amongst these except bio fuels all other forms of renewable energies are supplied as electricity. Hence, there is a great demand for development of efficient charge storage devices.

Till date the major contenders for energy storage applications are capacitors and batteries. They differ the way the energy is stored, the former involving chemical reactions between the electrolyte and electrode materials, whereas the later works on the principle of storage of electrostatic charge. This brings in a significant difference in their capabilities, the batteries have high energy density (higher wattage) and the capacitors have high power density (faster charging and long charge–discharge cycles). Of late the supercapacitors, popularly known as electrical double layer capacitors (EDLCs) or ultra-capacitors are gaining attention for energy storage applications. The supercapacitors (SC's)

are basically electrochemical capacitors with higher effective surface space and very small separation distances (0.3-0.5 nm) between the electrodes. Unlike the conventional capacitors, SC's do not contain a separate dielectric medium and the electric double layer's formed at the electrode-electrolyte interface acts as dielectric medium. Figure 1a illustrates the schematic representation of the electric double layer formation in the SC's. The categorization of these energy storage devices with respect to their power and energy densities are depicted in Figure 1b, which is referred as ragone plot. It is clearly evident that the capacitor possesses high power density with low energy density and in contrast the batteries possesses higher energy density with lower power density. In this context, SC's found to bridge the gap between capacitors and batteries. Growing demand for multitasking of electronic devices, especially smart phones, needs incorporation of various modules, which put restrictions on the size of battery. This in-turn affects its capacity and overall performance of the device. Hence, the SC's have a great advantage of storing high energy in minimum space and also works for longer charge-discharge cycles (few tens of thousands cycles) as the electrode does not get damaged, since they work on electrostatic means for charge storage without any chemical reactions. Moreover, the multitasking in smart devices demands

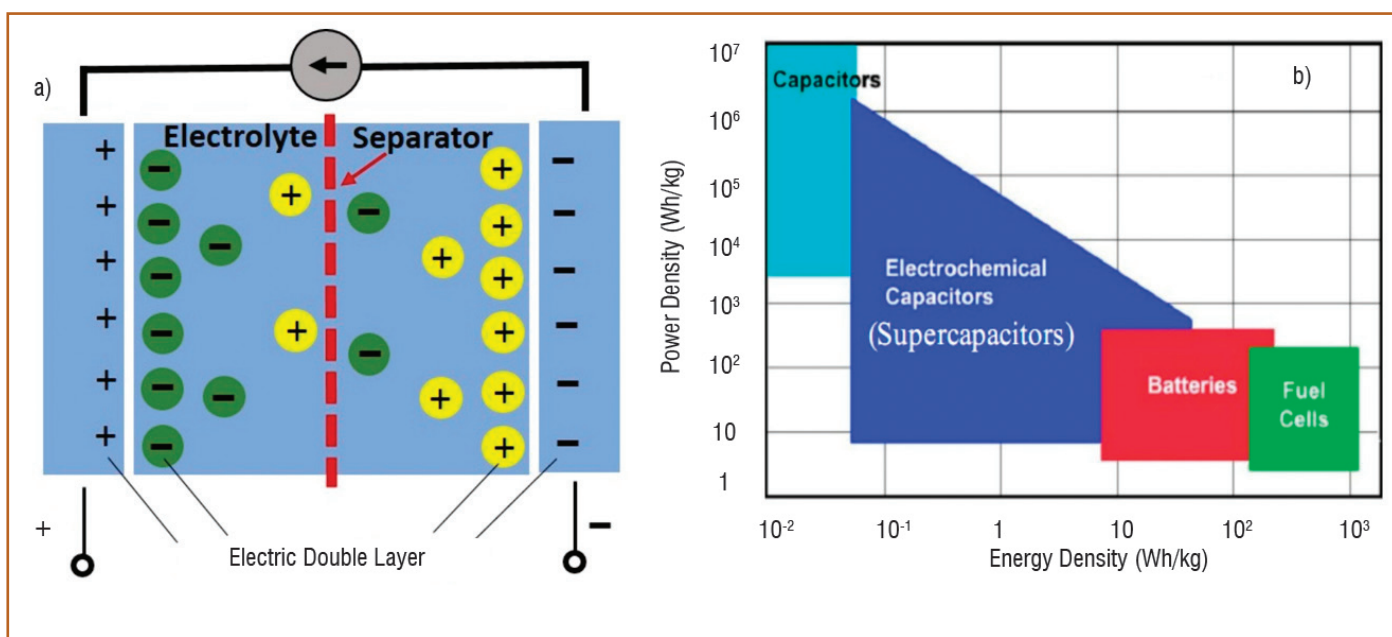


Figure 1: (a) Electric double layer formation in supercapacitors and (b) comparison of different energy storage devices

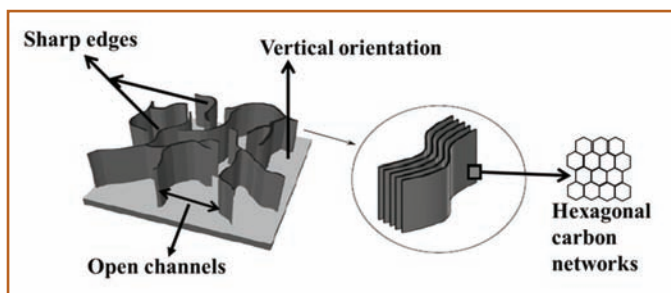


Figure 2: Schematic representation of the VGN morphology

high power in short durations, where the usage of SC's in combination with battery is an ideal solution. Therefore, SC's are viable alternate energy storage devices for both backup as well as protection against power disruptions.

The supercapacitors are further categorised based on their energy storage mechanism as: 1) electrical double layer capacitors (EDLC) that uses the coulombic charge accumulation of electric charge at the electrode electrolyte interface and 2) pseudo-capacitors (PC) involving reversible redox reactions at the electrode surface. Recently, the hybrid structures which are combination of both EDLC and PC are developed to achieve enhanced storage performance.

The EDLCs store energy either by electrostatically or by non-Faradically means by developing an electric double layer at the electrode surface. Recent advances in fabrication of nanostructures with different morphologies such as porous structures, nanorods/tubes and nanoflakes etc., facilitates the formation of electric double layers at different locations on the electrode surface. Due to the electrical continuity of the surfaces all the electrostatic energy gets coupled and thus EDLCs realizes higher energy densities than the conventional capacitors. Owing to their remarkable electrical conductivity, mechanical strength, chemical inertness, easy processing and wide range of operating temperatures, carbon materials are the most ideal candidate as EDLC SC's electrodes. A variety of carbon materials such as activated carbon (AC), carbon aerogels, carbon nanotubes (CNT's), carbon nanofibers etc., have been explored. In the process of fabrication of higher surface area materials, the meso porous materials and layered structures such as graphene received a lot of attention. Of late, the vertical graphene nanosheets (VGN) popularly known as graphene nanowalls or graphene flakes have also garnered the attention of researchers towards energy storage applications, due to their intriguing properties. Vertical graphene nanosheets are the ensemble of interconnected network of three-dimensional vertically standing few layer graphene sheets of few tens of nanometre thick. A schematic representation of

the 3D-interconnected VGN's networked structure is illustrated in Figure 2. This unique geometry bestows a large surface area and high density of sharp edges with non-stacking morphology. The 3D interconnected porous network of VGN structures also offer an easy access to its surfaces on both sides of the sheets for the electrolyte ions to interact with, which is a big boon for its utilization as an electrode material. Further, graphene based electrodes are inexpensive, lightweight and flexible with superior energy storage capacity. Thus, the VGN structures are being considered as an emerging material for energy storage applications.

Further, playing with the inter-sheet spacing, growth of secondary walls and vertical height of the sheets greatly influence the surface area of the VGN. Hence, VGN's with a controlled and optimized structure is essential to attain better capacitor performance. In general, as-grown VGN is highly hydrophobic in nature due to its jagged structure formed as a result of the interconnected porous 3D network as well as its hydrogen terminated edges. On the other hand, hydrophilic surfaces are the most desired ones for energy storage applications. Because, the electrolytic interactive area is the one that decides the energy storage capacity of electric double layer capacitors (EDLCs). The hydrophobic nature restricts the access of electrolyte ions to the interior surfaces of electrode materials which in-turn reduces the electrochemical interaction area, a crucial parameter to achieve high charge storage capacitance.

Surface modification methods like chemical activation and post-deposition plasma treatment are widely adopted methods to tune the wetting properties of nanostructures by altering the nature of defects and surface functional groups. However, chemical activation is time consuming and also there is a high possibility of damaging the morphology. Additionally, it is also difficult to achieve long lasting and stable super-hydrophilic surfaces through chemical activation process. Whereas, super-hydrophilicity achieved by post-deposition plasma treatment is quick and stable. It also preserves the geometry of the VGN, so that the crucial high surface area requirement is met.

At IGCAR, we have used a microwave assisted plasma enhanced chemical vapour deposition (PECVD) facility to grow VGN's on a variety of substrate materials ( $\text{SiO}_2/\text{Si}$ , Cu, Ni and carbon fibre sheet). The process conditions such as plasma power, substrate temperature, distance between substrate to plasma source, which are necessary to grow crystalline VGN's have been optimized. Ultra high pure (99.999%) argon (Ar) and methane ( $\text{CH}_4$ ) are used at an optimized ratio (5:1) for the VGN growth. The

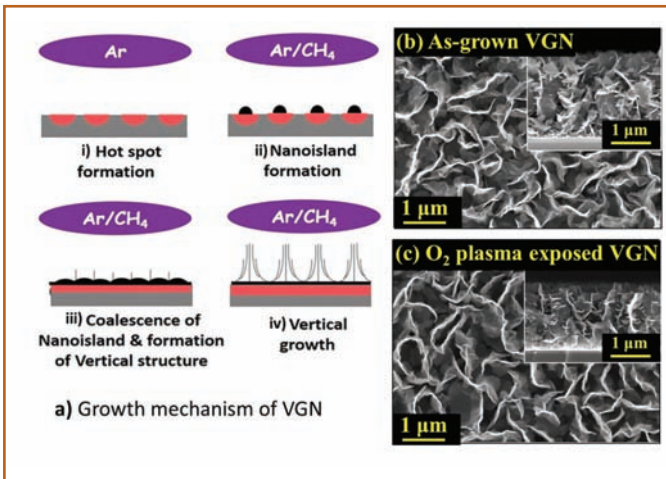


Figure 3: (a) Schematic of the VGN growth mechanism, (b) and (c) FESEM morphology with an inset of corresponding crosssection image of the as-grown and plasma treated VGN, respectively.

substrate temperature is maintained at 800°C and the optimum plasma power and substrate to plasma source distance are found to be 400 W and 30 cm, respectively.

The VGN growth mechanism established is shown as schematic in Figure 3a. During initial pre-cleaning process, the Ar plasma removes surface contaminations and creates localized hot spots or high temperature zones on substrate surface. These localized hot spots are the energetically most favourable regions to adsorb the hydrocarbon species. After the CH<sub>4</sub> gas is fed into the growth chamber, a variety of free radicals such as CH<sub>x</sub>, C<sub>x</sub>H<sub>y</sub>, C<sub>2</sub> dimers, Ar<sup>+</sup> and atomic hydrogen are expected to be created due to the high density plasma. These carbon and hydro-carbon radicals get adsorbed onto the hot spots due to surface diffusion and initiate rapid nucleation of nano-graphitic (NG) islands. As the growth continues, these islands coalesce and form a continuous interfacial NG base layer over the substrate. The coalescence of nano-islands during growth causes stress at the overlapping NG grain boundaries, whose release favours further nucleation and growth of graphene nanosheets in the vertical direction. Furthermore, the inbuilt electric field associated with the microwave assisted chemical vapour deposition technique is also found to influence the growth of graphene sheets in vertical direction.

Herein, the attempt to fabricate super-hydrophilic/super-wetting VGN structures without distorting its geometry using an in-situ oxygen plasma surface modification is elaborated. The post plasma treatment is carried out at 600W microwave power for 2 minutes. The enhanced charge storage performance of super-wetting VGN structures is demonstrated. Furthermore, a

correlation between wetting nature, oxygen functionalities and in-turn its influence on specific capacitance is established.

The field emission electron microscopy (FESEM) is employed to analyse the morphology and growth orientation of the as-grown as well as plasma-treated VGN's. Figures 3b and 3c depict morphology and crosssection view of both the as-grown as well as plasma exposed VGN's, respectively. Typical 3D-interconnected open networked structure and vertical oriented growth of VGN are confirmed by the FESEM analysis. It also showed the preservation of VGN geometry after plasma-treatment with a reduction in height. The VGN structure shows that the inter sheet spacing and vertical height are of a few micron's order.

The chemical structure and bonding of the VGN are examined using Raman spectroscopy and X-ray photoelectron spectroscopy (XPS), respectively. A typical Raman spectrum of the as-grown as well as plasma-treated VGN are shown in Figure 4a. Very trivial changes in the peak position of D, G and G' confirms insignificant damage to the graphitic structure due to the plasma-treatment. However, broadening of D and G peaks

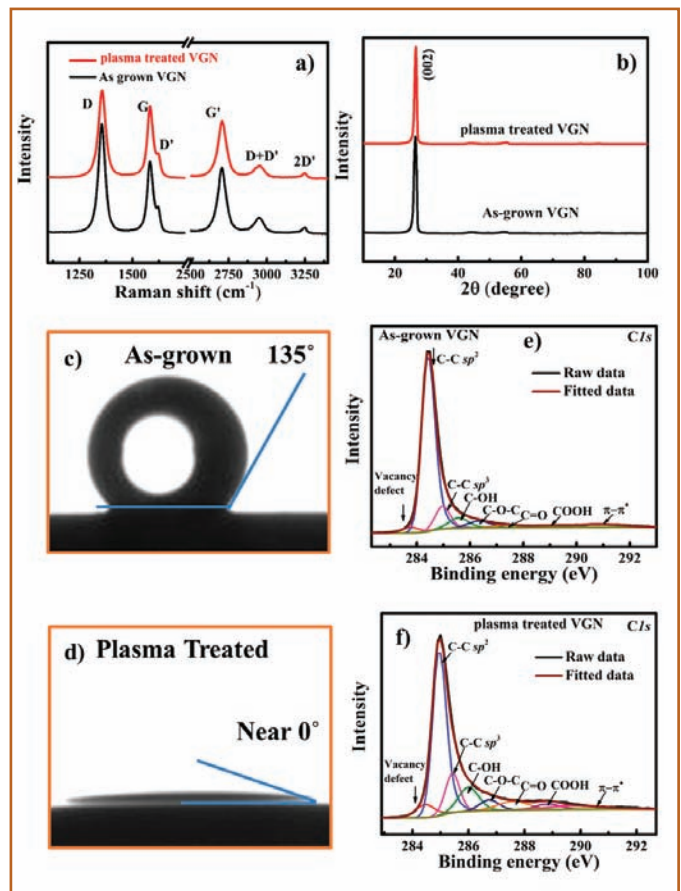


Figure 4: (a) Raman spectra, (b) X-ray profile, (c & d) water contact angle and (e & f) XPS spectra of as-grown and plasma-treated VGN, respectively

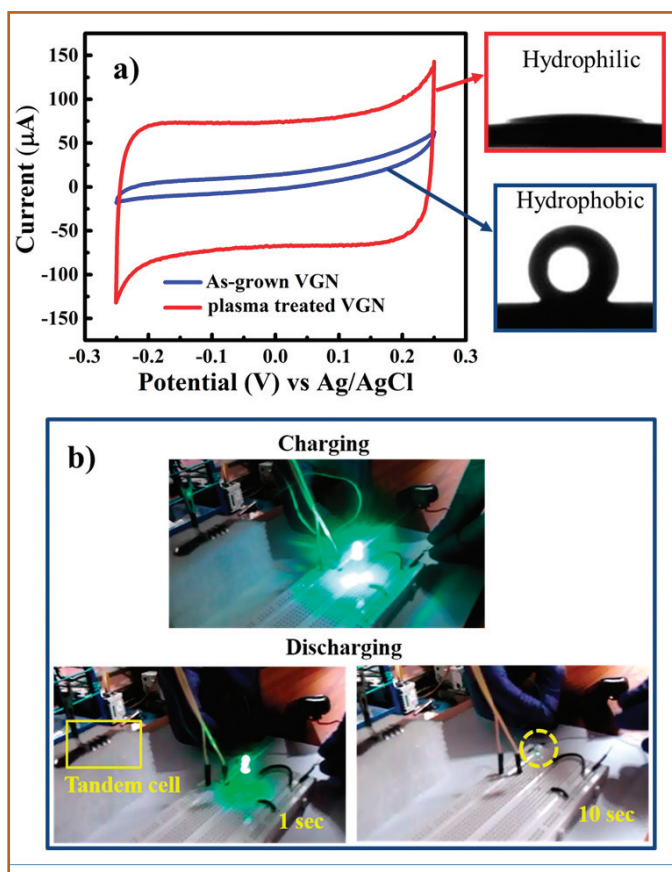


Figure 5: (a) Cyclic Voltammogram (CV) profile of as-grown and plasma-treated VGN and (b) LED testing of the tandem cell of VGN symmetric devices

along with reduction in both  $I_D/I_G$ , and  $I_G/I_G$  ratios are evident. The observed facts are attributed to the chemical etching due to oxygen plasma-treatment. The X-ray diffraction profile for the as-grown and plasma-treated VGN samples shown in Figure 4b affirms the structural stability, with unaltered characteristic diffraction peak of (002) at  $26.6^\circ$  corresponding to graphitic carbon. Water contact angle (WCA) measurements are carried out to confirm the transformation of highly hydrophobic as-grown VGN ( $135^\circ$ ) to super-hydrophilic (near  $0^\circ$ ) after oxygen plasma-treatment. The photograph of WCA shown in Figures 4c and 4d clearly evidenced the transformation in wetting nature of VGN's after plasma-treatment. To establish the correlation between wetting nature and surface functionalization XPS analysis was carried out. The deconvoluted C1s spectra of VGN depicted in Figures 4e & 4f affirmed the oxygen functional groups attachment to the VGN structures after plasma-treatment. It is also affirmed that the hydroxyl ( $-\text{OH}$ ) and carbonyl ( $-\text{C}=\text{O}$ ) type functionalities are enhanced after plasma exposure. A detailed comparison on the role of various plasma parameters on wetting nature of the VGN surface is given in our recent publications.

The supercapacitive performance of as-grown and plasma-treated VGN are evaluated by exposing a  $1 \times 1 \text{ cm}^2$  area to the KOH electrolyte in a 3-electrode system. The following equation is used to calculate the areal capacitance

$$C = \frac{\int I dV}{\Delta V.A.S}$$

where  $\int I dV$  represents area under the curve,  $\Delta V$  is the potential window,  $S$  is the scan rate (0.1 V/s) and  $A$  is the area of the electrode exposed to the electrolyte ( $1 \text{ cm}^2$ ). Figure 5a represents the cyclic voltammogram (CV) profiles of as-grown and plasma-treated VGN samples. A near rectangular CV profile and the linear charge-discharge curves signifies a good capacitive characteristic of the material. The increase in area under the CV after the plasma exposure confirms an enhancement in capacitance. The calculated value of capacitance for plasma-treated VGN is  $1.65 \text{ mF/cm}^2$  whereas for as-grown it is  $0.15 \text{ mF/cm}^2$ . The electrochemical impedance spectroscopy (EIS) is also carried out to bring out the insights on electrode-electrolyte interactions. The impedance spectra are fitted with an equivalent circuit model to obtain the equivalent series resistance ( $R_s$ ) and the measured values are found to be  $2.56$  and  $1.75 \Omega$  for as-grown and plasma-treated VGN, respectively. Additionally, for porous materials and open networked structures the electrochemical active surface area plays an important role than the actual surface area. Hence, we calculated the electrochemical active surface area from the capacitive current ( $|I_d|$ ) vs. scan rate (V/s). The active surface area is calculated using 'Jellium model' and the measured values are found to be  $8.5 \text{ m}^2/\text{g}$  for as-grown and  $160 \text{ m}^2/\text{g}$  for plasma-treated VGN, respectively. These findings clearly evidenced the significant role of surface functionalities, surface area and hydrophilicity on the energy storage capacity. Finally, a symmetric electrochemical capacitor device is fabricated using in-situ plasma-treated VGN electrodes. The LED test is carried out on the tandem cell prepared by connecting the symmetric devices in series to check the potentiality of these devices. The tandem cell is charged up to 4 V, Figure 5b inset shows the LED glows at different times. These findings paved way to extend the potential utilization of oxygenated VGN structures for energy storage applications.

S. R. Polaki and colleagues  
Materials Science Group

## Young Officer's FORUM

### Low Cycle Fatigue-High Cycle Fatigue Interaction in Type 316LN Stainless Steel

Most of the current investigations pertaining to the fatigue behavior of structural materials are dedicated to isolated events of Low Cycle Fatigue (LCF) or High Cycle Fatigue (HCF) loading. In Sodium Cooled Fast Reactors (SFRs), most of the components operating at high temperatures are subjected to heating and cooling transients (sharp thermal gradients from surface to core of thick components) during startup and shutdown. This induces thermal stresses in the material, if thermal strain (expansion/contraction) is totally/partially constrained. Repetition of such thermal stresses causes low cycle fatigue damage in the component. Random temperature fluctuations in the mixing region of hot and cold sodium, known as thermal stripping lead to high cycle fatigue damage on the adjoining metal wall surfaces. Cyclic variations of temperature caused by fluctuation of stratified sodium layers also result in HCF damage. These damages are predominant on the core cover plate in the main vessel and tee junctions in the secondary sodium pipelines (thermal striping) and inner vessel (thermal stratification). Oscillations in the sodium free level in the main vessel during steady state operation and flow induced vibrations in the IHX (intermediate heat exchanger) are also potential sources of HCF damage. The presence of HCF cycling at locations where LCF is significant is the most damaging scenario since HCF damage gets superimposed on the LCF, leading to strong LCF-HCF interactions. This calls for a detailed investigation into the mechanism of LCF-HCF interaction to ensure better structural design of SFR components. Towards this objective, a detailed investigation was carried out on high temperature LCF-HCF interaction in a type 316LN austenitic stainless steel (the main structural material for the in-vessel components of SFRs) in the temperature range of 823-923 K which encompasses the operating temperature as well as that of power transients in SFRs. Towards investigating the LCF-HCF interaction behavior of the alloy, specimens were initially exposed to prior LCF deformation at different LCF strain amplitudes ( $\pm 0.25\%$  -  $\pm 0.6\%$ ) for various life



Dr. Aritra Sarkar working in the Fatigue Studies Section, MMG, IGCAR is from the 53<sup>rd</sup> batch of BARC Training school, Mumbai. He has acquired M.Tech degree in Metallurgy from HBNI and Ph.D (Doctor of Engineering) from Nagaoka University of Technology, Japan in 2018 through JSPS RONPAKU fellowship. Dr. Aritra Sarkar is actively involved in characterizing deformation mechanisms under high temperature ratcheting as well as damage interaction under low cycle fatigue & high cycle fatigue on austenitic stainless steels, which are critical issues for the reliability of the sodium cooled fast reactor (SFR). He has 25 journal publications to his credit along with numerous awards like Outstanding M. Tech thesis award, DAE group achievement awards and JSPS medal for his Ph.D.

fractions in the range, 20-80%. The pre-cycled specimens were subsequently subjected to HCF loading up to fracture.

#### Effect of prior LCF Cycling on HCF Behavior: LCF-HCF Interaction

The variations of remnant HCF life with prior LCF exposure, in the range 20-80% for the three different strain amplitudes are shown in Figure 1. The specimens pre-cycled in LCF showed a decrease in the residual HCF life which became more prominent with an increase in the LCF exposure. The LCF pre-cycling was found to intensify the fatigue damage taking place during HCF loading, which leads to strong interaction between LCF and HCF. The term "damage" in the present case is denoted as material degradation under fatigue,

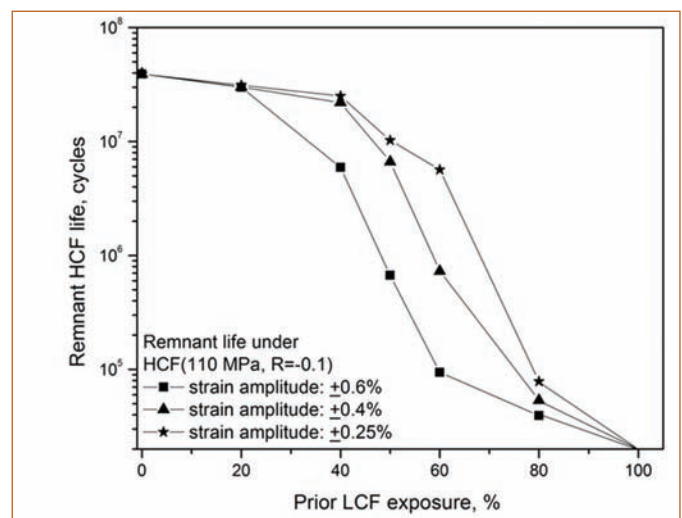


Figure 1: Variation of remnant HCF lives with prior LCF exposure (%) for different strain amplitudes ranging from  $\pm 0.25\%$  to  $\pm 0.6\%$ , 923 K

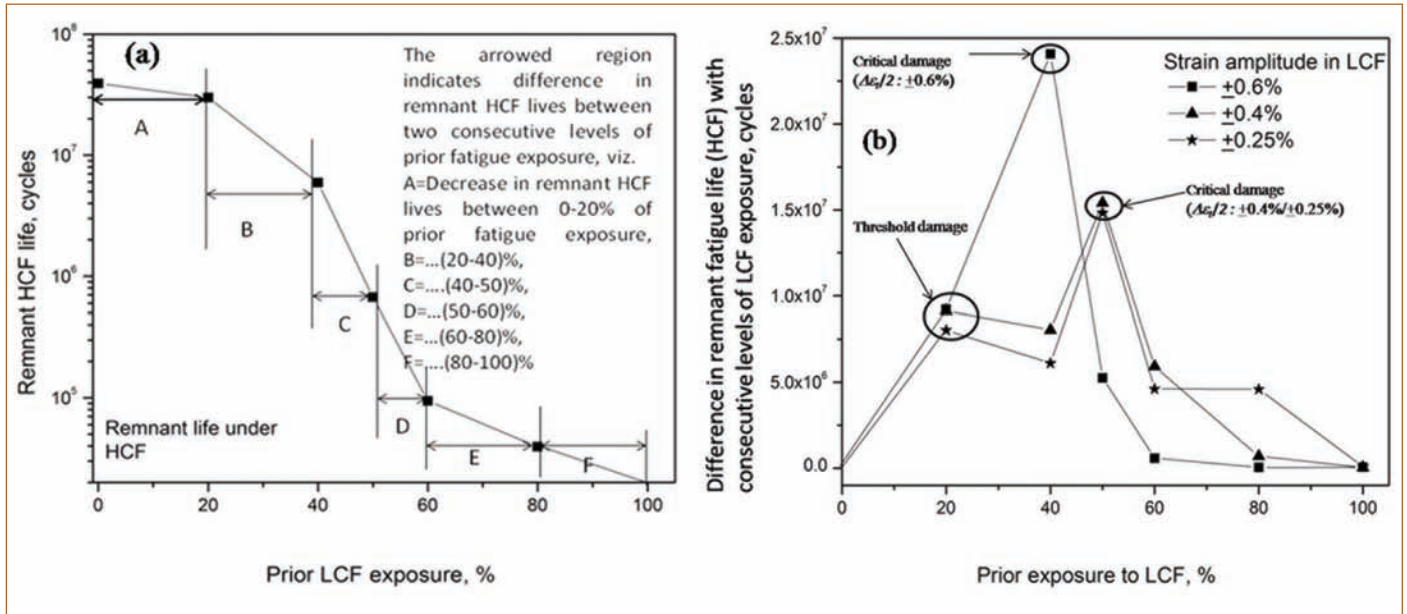


Figure 2: (a) Schematic illustrating the method of calculating the difference in remnant HCF lives between two consecutive levels of prior LCF exposures, (b) Variation of difference in remnant fatigue lives between different levels of prior LCF exposure with degree of prior LCF exposure, 923 K

through initiation and propagation of cracks, ultimately causing fracture. Prior crack initiation under LCF cycling serves to bring down the remnant HCF life by shortening the crack initiation phase under HCF.

Even though remnant HCF life follows a decreasing trend with increase in prior LCF fraction which was consistent for all three strain amplitudes (Figure 1), the magnitude of remnant lives varies widely with prior LCF exposure as well as applied strain amplitude. This indicates that both strain amplitude and exposure to prior LCF had strong influence on the remnant HCF lives. This was brought out more clearly by plotting the difference (drop) in remnant HCF lives between two consecutive levels of prior LCF exposure (values A-F shown through the schematic in Figure 2a with the degree of prior LCF exposure (Figure 2b). Comparatively insignificant change in remnant HCF lives after prior LCF cycling between 0 - 20% is mainly attributed to the minimal LCF damage accrued within that span of LCF life. This suggests that there was no significant LCF-HCF interaction within this LCF pre-exposure. Moreover, up to around 20% prior LCF cycling, the variation in the difference in remnant HCF lives with respect to the three different strain amplitudes was found to be only marginal. This indicates that a threshold damage under LCF is necessary for initiation of an appreciable LCF-HCF interaction, for which the remnant HCF lives will be a weak function of strain amplitude. However, the difference in reductions in the

remnant HCF lives varied widely with respect to strain amplitude as LCF pre-exposure is increased beyond threshold damage, demonstrating strong strain amplitude dependency. Further, the magnitude of decrease in the remnant HCF life between different degrees of prior LCF cycling is quite substantial with increase in LCF pre-exposure beyond threshold damage, which essentially implies that strong LCF-HCF interaction is taking place. The difference in HCF life was found to reach its maximum between 20% - 40% of LCF life and between 40%-50% of LCF life for  $\Delta\epsilon_r/2: +0.6\%$  and  $\Delta\epsilon_r/2: +0.4/+0.25\%$  respectively. This indicates that the rate of damage accumulation was highest between the above LCF exposures. In other words, LCF-HCF interaction was strongest for a LCF pre-exposure of 20-40% at  $\Delta\epsilon_r/2: +0.6\%$  and 40-50% at  $\Delta\epsilon_r/2: +0.4/+0.25\%$ . This also suggests that there is a critical damage under LCF (occurring at 40% LCF pre-exposure at  $\Delta\epsilon_r/2 = \pm 0.6\%$  and 50% LCF pre-exposure at the lower strain amplitudes) for which the LCF-HCF interaction is most effective. This critical damage thus varied inversely with the applied  $\Delta\epsilon_r/2$  employed in LCF pre-cycling. Hence, the window for effective LCF-HCF interaction shifts towards the right with a decrease in the applied strain amplitude (as reflected from Figure 2b). The mechanism of LCF-HCF interaction is mainly based on difference in crack initiation and propagation under LCF and HCF respectively. Under LCF conditions, multiple micro-cracks will initiate at the surface

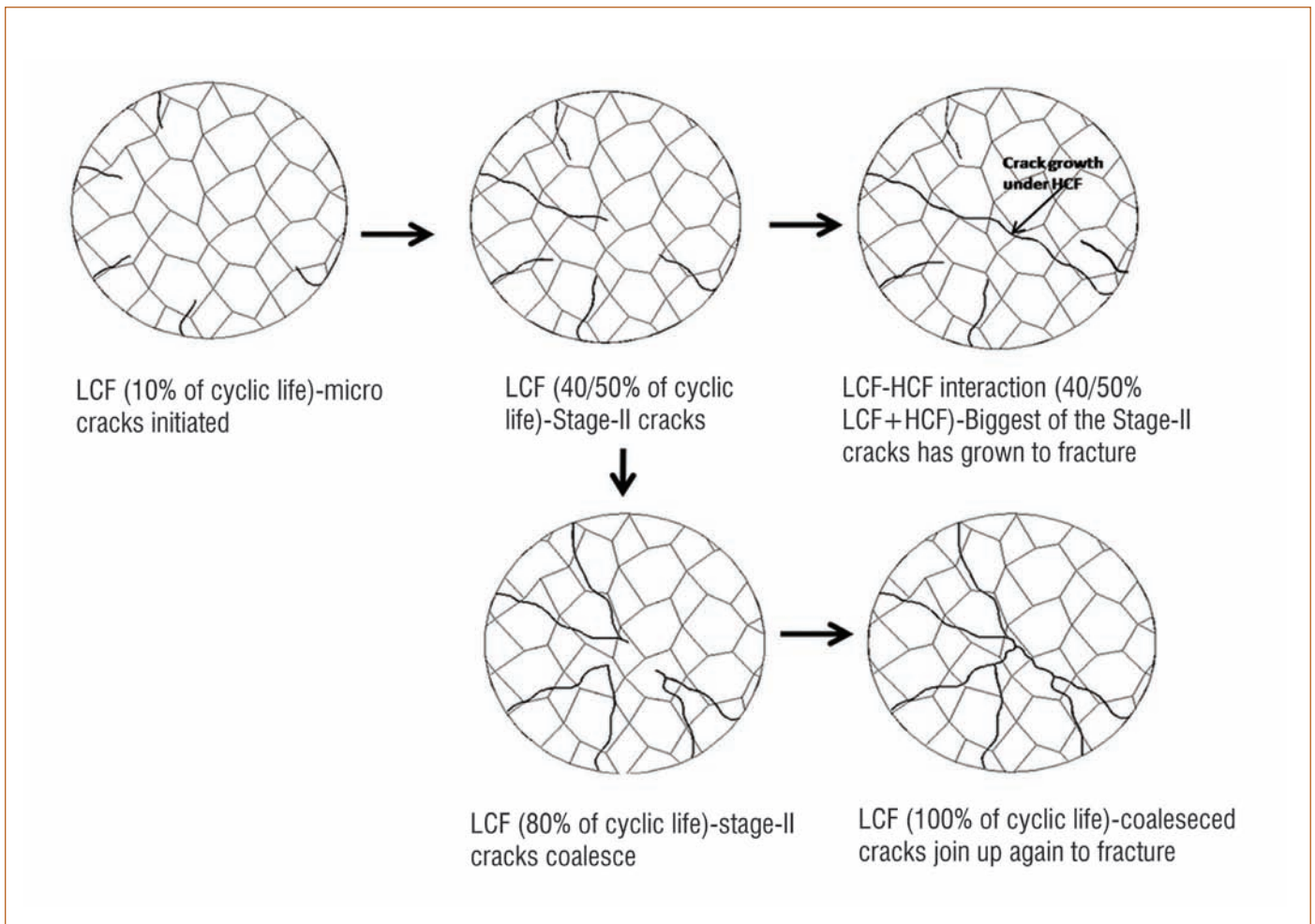


Figure 3: Schematic showing mechanism of LCF-HCF interaction based on initiation and propagation of cracks

and grow to the extent of Stage-II cracks with successive cycling. The transition from Stage-I to Stage-II crack is a function of the applied stress/strain and will take place early during LCF compared to HCF. Under continuous cycling (LCF), these cracks coalesce among themselves to form a macro crack leading to final failure. However, an interruption in the LCF stage followed by HCF cycling at a lower stress hinders the coalescence of such Stage-II cracks with the result that only the longest of the cracks initiated under pre-LCF deformation will grow further during the HCF phase. This is the ideal condition for the occurrence of critical damage (maximum LCF-HCF interaction) (shown schematically in Figure 3). At lower  $\Delta\varepsilon_c/2$ , number of crack initiation sites will be lower compared to higher strain amplitudes like  $\Delta\varepsilon_c/2: +0.6\%$ . Hence, formation of Stage-II cracks satisfying the condition for occurrence of critical damage will be reached at a higher prior LCF exposure. Thus, LCF-HCF interaction is a strong function of both the degree and the

strain amplitude of prior LCF exposure; an optimum combination of the above two factors seems necessary for the appearance of the same. Hence, critical damage can be considered as an important design criterion to identify the safe and unsafe regions under LCF-HCF interaction and the combination of strain amplitude and prior LCF exposure corresponding to the critical damage must be avoided in practice. The concept of critical damage was also further explored from fracture mechanics point of view to identify a critical crack length ( $a_{cr}$ ) which can serve as an important parameter under LCF-HCF interaction considering the fact that fracture mechanics can be applied for remaining life estimation only when this critical value is reached.

Aritra Sarkar  
Metallurgy & Materials Group

## Young Researcher's FORUM

# Spectroscopic Investigations on the Coordination Environment of Uranyl Ion in Ionic Liquid Medium



G. Murali Krishna, is pursuing Ph.D under HBNI in Irradiated Fuel Studies Section of Fuel Chemistry Division, MC&MFCG, IGCAR. He has Completed M. Sc. from Andhra University, Vishakapatnam. The main areas of interest are electrochemical studies of actinides and lanthanides in ionic liquid medium and spectroscopic investigation of metal complexes in ionic liquid medium. He has six peer reviewed journal publications.

Application of room temperature ionic liquids (RTILs) is receiving increased attention in the recent past in the area of nuclear fuel reprocessing and waste management. RTILs are organic salts with melting points lower than 373 K. The attractive properties of ionic liquids suitable for nuclear fuel cycle application are: tunable nature to dissolve a wide variety of extractants, negligible vapour pressure as compared to the conventional diluents, extraordinary extraction of metal ions with high separation factor from interferences, wide electrochemical window for the electrodeposition of actinides, etc. The Extraction-Electrodeposition (EX-EL) approach developed in our laboratory exploits the wide electrochemical window and hydrophobicity of the ionic liquid to separate the metal ion from aqueous wastes by a solvent extraction procedure, and recover the extracted metal in a convenient solid form, by electrodeposition from the ionic liquid phase. In this context, the EX-EL approach has been demonstrated for the recovery of uranium as uranium oxide and the fission product palladium as metallic palladium from nitric acid solutions, using ionic liquid as a medium, in our laboratory.

The extraction of metal ions from aqueous phase electrodeposition of the metal ion into metallic form at the working electrode is governed by the nature of the species diffusing across the liquid-liquid interphase during extraction and across liquid-solid interphase during electrodeposition. This in turn depends on the size and strength of the ligand coordinated to the metal ion. Generally, it is observed that strong complexing ligands facilitate extraction but lowers the diffusion of electroactive species during electrodeposition. The electrode reaction happening at the working electrode is very complex and highly irreversible in the presence of ligands. In view of this, it is necessary to understand the coordination behavior of the metal ion in the presence of ligands that are present in ionic liquid medium.

To understand the coordination environment of uranyl ion obtained after the extraction of uranyl nitrate from nitric acid medium in a solution of tri-n-butyl phosphate in 1-butyl-3-methylimidazolium bistrifluoromethanesulfonylimide ( $C_4mimNTf_2$ ) ionic liquid, the visible absorption spectrum of uranyl nitrate in  $C_4mimNTf_2$  at U: $NO_3$ :TBP mole ratio of 1:2:2 was recorded and displayed in

Figure 1. The spectrum of uranyl nitrate in TBP/ $C_4mimNTf_2$  is characterised by the presence of fine structure bands at 428, 440, 451 and 465 nm. The intensity of other bands is less. The visible absorption spectrum of uranyl nitrate in TBP/ $C_4mimNTf_2$  matches well with the absorption spectrum of uranyl nitrate in 14 M nitric acid which is also shown in the same Figure. At 14 M nitric acid, majority of uranyl ions exist as neutral  $UO_2(NO_3)_2$  complex. The similarity in the absorption bands indicates that the overall structure of uranyl nitrate specie in ionic liquid medium is not affected significantly by the addition of TBP. Therefore, it is quite likely that uranyl nitrate in ionic liquid medium is essentially solvated by TBP in the outer coordination sphere and exists as  $UO_2(NO_3)_2(TBP)_2$  in  $C_4mimNTf_2$  medium. Since  $NTf_2^-$  of ionic liquid is relatively big and is a weak field ligand as compared to nitrate, it does not participate in coordination with  $UO_2^{2+}$  ion in the presence of nitrate.

Since the  $UO_2(NO_3)_2(TBP)_2$  is quite big, the diffusion of uranyl nitrate species towards the working electrode during electrodeposition

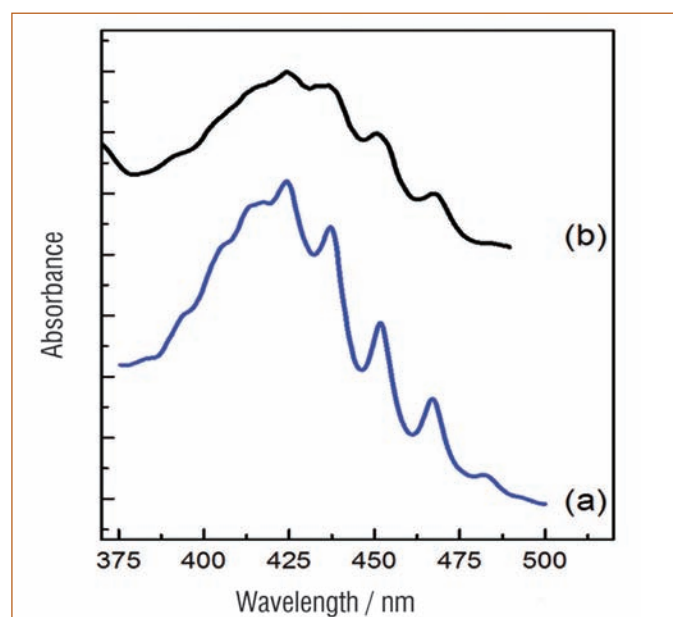


Figure 1: UV-Visible absorption spectrum of (a) 80 mM  $UO_2(NO_3)_2$  dissolved in  $C_4mimNTf_2$  containing TBP (160 mM) and (b) 80 mM  $UO_2(NO_3)_2$  dissolved in 14 M  $HNO_3$

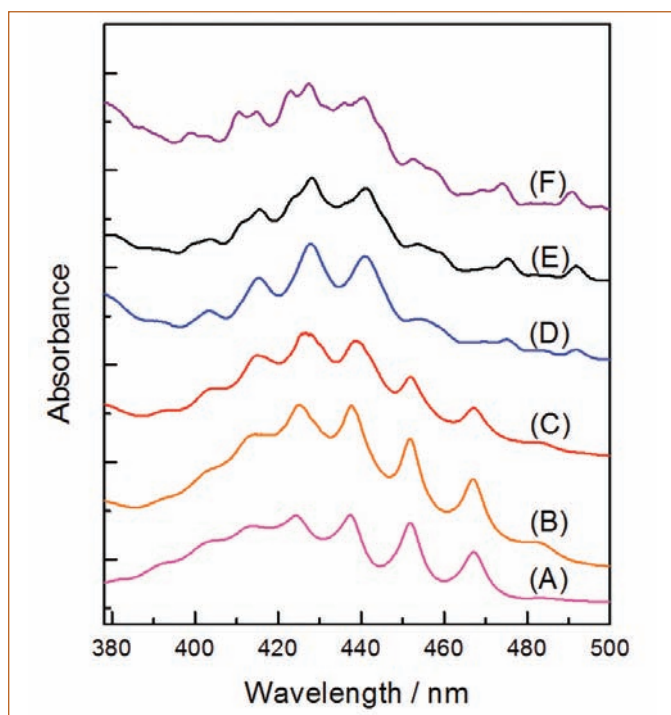
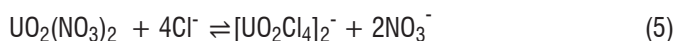
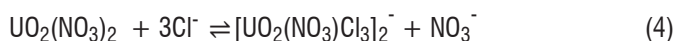
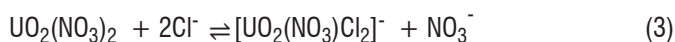
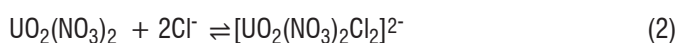
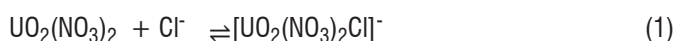


Figure 2: UV-Visible absorption spectrum of 80 mM  $\text{UO}_2(\text{NO}_3)_2$  dissolved in  $\text{C}_4\text{mimNTf}_2$  containing TBP (160 mM), in the presence and absence of  $\text{C}_4\text{mimCl}$ . The mole ratio of U :  $\text{NO}_3$  : TBP : Cl is 1 : 2 : 2 : 0 in (A), 1 : 2 : 2 : 1 in (B), 1 : 2 : 2 : 2 in (C), 1 : 2 : 2 : 4 in (D) and 1 : 2 : 2 : 6 in (E)

could be difficult. However, if the TBP is decomplexed from the outer coordination sphere and the nitrite present in the inner coordination sphere is substituted by simple anions such as  $\text{Cl}^-$ , it is quite likely that the diffusion of the resultant complex perhaps could be improved. In this direction the coordination environment of uranyl ion in presence of  $\text{Cl}^-$  ion was investigated and the results are discussed below.

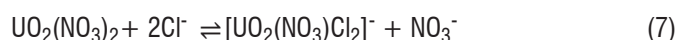
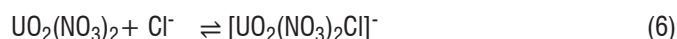
Figure 2 shows the visible-absorption spectrum of uranyl species at various mole ratios of U :  $\text{NO}_3$  : TBP : Cl. In all the cases the U :  $\text{NO}_3$  : TBP mole ratio was maintained constant at 1 : 2 : 2. It can be seen that the addition of  $\text{Cl}^-$  ions decreases the intensity of fine structure bands at 451, 467 and 482 nm and increases the intensity of 403, 415 and 423 nm bands. When the mole ratio of U :  $\text{NO}_3$  : TBP : Cl is 1 : 2 : 2 : 4, a couple of new bands at 457 nm and 475 nm emerge and become prominent when the mole ratio of U :  $\text{NO}_3$  : TBP : Cl reaches 1 : 2 : 2 : 6. In addition, the shape of the absorption fine structure is further broadened at 1 : 2 : 2 : 6 (U :  $\text{NO}_3$  : TBP : Cl) mole ratio. The following reactions can be proposed for the complexation of neutral uranyl nitrate with chloride ion.



It should be noted that the abundance of various uranyl species in  $\text{C}_4\text{mimNTf}_2$  medium depends upon relative mole ratio of U :  $\text{NO}_3$  : Cl, and on the relative stability of the resultant complex in ionic liquid medium. Comparing the visible spectrum obtained in the present study with those reported in the literature, our results confirmed that most dominant specie was  $[\text{UO}_2(\text{NO}_3)_2\text{Cl}]^-$  at U :  $\text{NO}_3$  : Cl mole ratio of 1:2:1 and at higher Cl : U ratio (4 or higher), the uranyl ion forms mixture of complexes such as  $[\text{UO}_2\text{Cl}_3(\text{NO}_3)]^{2-}$  and  $[\text{UO}_2\text{Cl}_4]^{2-}$ . Since TBP is a neutral and a weak field ligand as compared to  $\text{NO}_3^-$  and  $\text{Cl}^-$ , it is not likely to be involved in coordination with these anionic uranyl species.

#### Raman Spectroscopy of "Free" Nitrate

The equations (1) to (5) indicates that the addition of  $\text{Cl}^-$  ions to  $\text{UO}_2(\text{NO}_3)_2$  in  $\text{C}_4\text{mimNTf}_2$  results in the substitution of nitrate ion by  $\text{Cl}^-$  ions. The nitrate ion released from uranyl coordination sphere can be easily monitored by the  $\text{NO}_3^-$  symmetric stretching bands in Raman spectroscopy at  $1042\text{ cm}^{-1}$ . For instance, when the U :  $\text{NO}_3$  : Cl mole ratio is 1 : 2 : 1 the following reactions could be possible.



The added  $\text{Cl}^-$  stoichiometrically reacts with uranyl nitrate leading to the formation of  $[\text{UO}_2(\text{NO}_3)_2\text{Cl}]^-$  or the uranyl nitrate present in the solution is partially converted to  $[\text{UO}_2(\text{NO}_3)\text{Cl}_2]^-$ . During partial conversion the unreacted  $\text{UO}_2(\text{NO}_3)_2$  remains in ionic liquid. Among these two reactions, the reaction (7) results in the release of nitrate ion from uranyl coordination sphere. Monitoring the liberated "free" or "unco-ordinated" nitrate ion in Raman spectrum at  $1042\text{ cm}^{-1}$  would provide more insights into the feasibility of the above reactions and the abundance of uranyl species.

Figure 3 shows the Raman spectrum of uranyl ion at U: $\text{NO}_3$ :TBP:Cl mole ratio ranging from 1 : 2 : 2 : 0 to 1 : 2 : 2 : 6. It can be seen that the "free" nitrate bands at  $1042\text{ cm}^{-1}$  are not present, in the absence of  $\text{Cl}^-$  ion i.e., at 1 : 2 : 2 : 0 mole ratio as well as at 1 : 2 : 2 : 1 mole ratio. This indicates that  $\text{NO}_3^-$  ion is not "free" in both cases. The absence of "free" nitrate ion peak in the Raman spectrum indicates that the dominant uranyl specie is  $[\text{UO}_2(\text{NO}_3)_2\text{Cl}]^-$  in ionic liquid medium at 1 : 2 : 2 : 1 mole ratio. At 1 : 2 : 2 : 2 mole ratio of U :  $\text{NO}_3$  : TBP : Cl, the reactions shown in (2) and (3) are possible. The Raman spectrum of the ionic liquid solution at 1 : 2 : 2 : 2 mole ratio, shows the presence of a new absorbance band at  $1042\text{ cm}^{-1}$  indicating the presence of "free" nitrate ion in ionic liquid medium. This nitrate ion could have been liberated from uranyl ion coordination sphere possibly by the reactions shown in equation (3). This indicates that the dominant uranyl specie at 1 : 2 : 2 : 2 mole ratio is likely to be  $[\text{UO}_2(\text{NO}_3)\text{Cl}_2]^-$ . It is also noted that increasing the concentration of  $\text{Cl}^-$  ions increases the intensity of  $1042\text{ cm}^{-1}$  band. This indicates the sequential substitution of  $\text{NO}_3^-$  ions present in the uranyl coordination sphere by  $\text{Cl}^-$  ions by the reactions shown in equations (4) and (5). All these observations

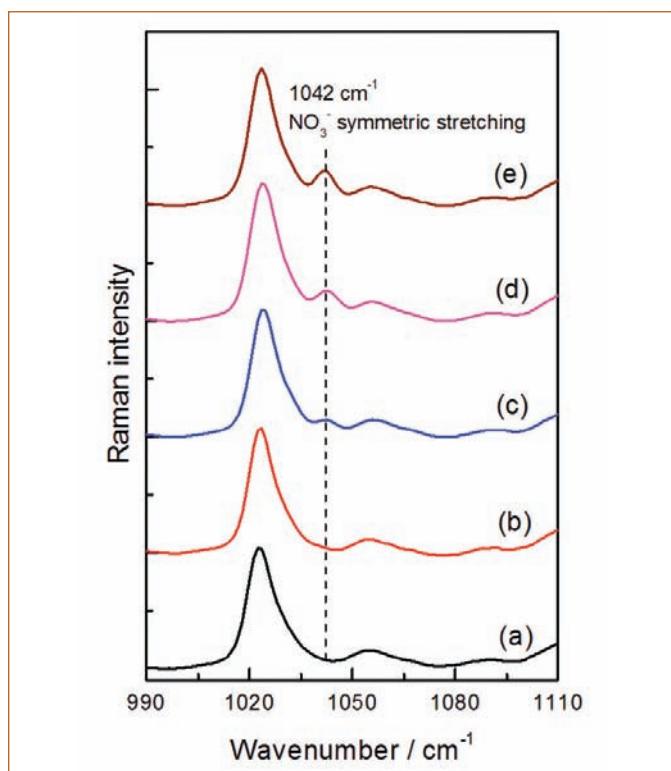


Figure 3: Raman spectrum of 80 mM  $\text{UO}_2(\text{NO}_3)_2$  dissolved in  $\text{C}_4\text{mimNTf}_2$  containing TBP (160 mM), in the presence and absence of  $\text{C}_4\text{mimCl}$ . The mole ratio of U :  $\text{NO}_3$  : TBP : Cl is 1 : 2 : 2 : 0 in (a), 1 : 2 : 2 : 1 in (b), 1 : 2 : 2 : 2 in (c), 1 : 2 : 2 : 4 in (d), 1 : 2 : 2 : 6 in (e).

confirm that  $[\text{UO}_2(\text{NO}_3)_2(\text{TBP})_2]$  present in ionic liquid medium is gradually converted to various anionic species by the addition of  $\text{C}_4\text{mimCl}$ , and the abundance of various uranyl species increases in the order from reaction (1) to (5) with increase in the mole ratio of  $\text{Cl}^-$  ion in the solution. At higher mole ratio of U :  $\text{NO}_3$  : TBP : Cl, i.e., at 1 : 2 : 2 : 6, the dominant species likely to be present in the solution is  $[\text{UO}_2\text{Cl}_4]^{2-}$ .

#### Raman Spectroscopy of U=O Stretching

The gradual substitution of  $\text{NO}_3^-$  ions present in the uranyl ion coordination sphere by  $\text{Cl}^-$  ions can also be monitored by recording the position of U=O stretching bands in the Raman spectrum. In Raman spectrum, the uranyl nitrate can be easily identified by the presence of an absorption band at  $860\text{ cm}^{-1}$  and that of chlorocomplex,  $[\text{UO}_2\text{Cl}_4]^{2-}$  by the absorption bands at  $830\text{ cm}^{-1}$ . Figure 4 shows the Raman spectrum of uranyl species at various mole ratios of U :  $\text{NO}_3$  : TBP : Cl varied from 1 : 2 : 2 : 0 to 1 : 2 : 2 : 6. The Raman spectrum shows the presence of an absorption band at  $860\text{ cm}^{-1}$ , which is characteristic to uranyl nitrate as expected at 1 : 2 : 2 : 0 mole ratio. The absorption band at  $830\text{ cm}^{-1}$  is due to the ionic liquid,  $\text{C}_4\text{mimNTf}_2$ . It is to be noted that the relative intensity at wave numbers 860 and  $830\text{ cm}^{-1}$  are comparable at 1 : 2 : 2 : 0 mole ratio. The addition of  $\text{Cl}^-$  ion to  $\text{UO}_2(\text{NO}_3)_2(\text{TBP})_2$  solution results in the gradual shift of  $860\text{ cm}^{-1}$  to lower frequency region. At 1 : 2 : 2 : 1 mole ratio of U :  $\text{NO}_3$  : TBP : Cl, the  $860\text{ cm}^{-1}$  absorption

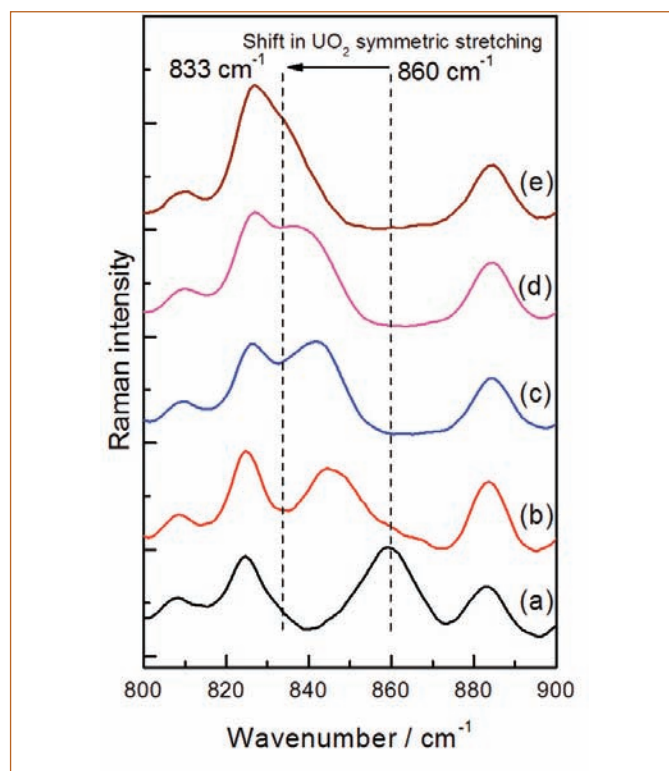


Figure 4: Raman spectrum of 80 mM  $\text{UO}_2(\text{NO}_3)_2$  dissolved in  $\text{C}_4\text{mimNTf}_2$  containing TBP (160 mM), in the presence and absence of  $\text{C}_4\text{mimCl}$ . The mole ratio of U :  $\text{NO}_3$  : TBP : Cl is 1 : 2 : 2 : 0 in (a), 1 : 2 : 2 : 1 in (b), 1 : 2 : 2 : 2 in (c), 1 : 2 : 2 : 4 in (d), 1 : 2 : 2 : 6 in (e).

band is partially shifted to  $850\text{ cm}^{-1}$  and the original band at  $860\text{ cm}^{-1}$  appears as a shoulder to the  $850\text{ cm}^{-1}$  band. The presence of a weak shoulder at  $860\text{ cm}^{-1}$  indicates that  $\text{UO}_2(\text{NO}_3)_2(\text{TBP})_2$  is still present in the solution, possibly with low abundance. However, the dominant species seems to be  $[\text{UO}_2(\text{NO}_3)_2\text{Cl}]^-$  at 1 : 2 : 2 : 1 mole ratio. Further addition of  $\text{Cl}^-$  ion, shifts the position of U=O stretching bands to  $830\text{ cm}^{-1}$ , with negligible intensity at  $860\text{ cm}^{-1}$ . This indicates that the abundance of  $\text{UO}_2(\text{NO}_3)_2(\text{TBP})_2$  species is negligible at U :  $\text{NO}_3$  : TBP : Cl mole ratio of 1 : 2 : 2 : 2. The intensity of  $830\text{ cm}^{-1}$  (due to ionic liquid) and  $850\text{ cm}^{-1}$  (due to U=O stretching) at 1 : 2 : 2 : 2 mole ratio are equal in this case. At 1 : 2 : 2 : 4 mole ratio of U :  $\text{NO}_3$  : TBP : Cl, the U=O stretching bands are shifted further from  $850\text{ cm}^{-1}$  to  $840\text{ cm}^{-1}$  and appears as a shoulder to the  $830\text{ cm}^{-1}$  band. At 1 : 2 : 2 : 6 mole ratio, the U=O band completely merges with the ionic liquid band at  $830\text{ cm}^{-1}$ . Further addition of  $\text{Cl}^-$  did not shift the position of  $830\text{ cm}^{-1}$  band further. Therefore, the study indicates that uranyl nitrate-TBP complex is gradually converted to various chloro complexes with the addition of  $\text{C}_4\text{mimCl}$ . At 1 : 2 : 2 : 1 mole ratio of U :  $\text{NO}_3$  : TBP : Cl, majority of the uranium species exists as  $[\text{UO}_2(\text{NO}_3)_2\text{Cl}]^-$  with residual  $[\text{UO}_2(\text{NO}_3)_2(\text{TBP})_2]$  and at 1 : 2 : 2 : 6 mole ratio and above, the dominant uranium species is  $[\text{UO}_2\text{Cl}_4]^{2-}$ .

#### ATR-FTIR Spectroscopy of U=O Stretching

The formation of chloro complexes of uranium in  $\text{C}_4\text{mimNTf}_2$  can

be further evidenced by probing the transmittance bands of U=O stretching frequencies by FTIR spectroscopy. The position and shift of U=O and P=O (of TBP) stretching bands with the addition of Cl<sup>-</sup> ions was probed by ATR-FTIR spectroscopy. However, it was found that the region from 1500 to 800 cm<sup>-1</sup> was completely masked by the strong transmittance bands of the ionic liquid, C<sub>4</sub>mimNTf<sub>2</sub>. In view of this, it was necessary to correct the spectrum of the sample with respect to the C<sub>4</sub>mimNTf<sub>2</sub> background and present as the differential ATR-FTIR spectrum of the sample. In fact, this kind of background correction was possible due to the availability of ATR in FTIR-spectrometer. Figure 5 shows the differential ATR-FTIR spectrum of UO<sub>2</sub>(NO<sub>3</sub>)<sub>2</sub> in C<sub>4</sub>mimNTf<sub>2</sub>. The uranyl nitrate spectrum was corrected with respect to the spectrum of C<sub>4</sub>mimNTf<sub>2</sub> and presented as differential spectrum in Figure 5. The corrected spectrum shows the presence of transmittance bands at 950 cm<sup>-1</sup>. This indicates that UO<sub>2</sub><sup>2+</sup> is co-ordinated to nitrate ions in the form of UO<sub>2</sub>(NO<sub>3</sub>)<sub>2</sub> in ionic liquid medium. The addition of TBP to UO<sub>2</sub>(NO<sub>3</sub>)<sub>2</sub>/C<sub>4</sub>mimNTf<sub>2</sub>, at U : NO<sub>3</sub> : TBP mole ratio of 1 : 2 : 2, results in the shift of O=U=O asymmetric stretching bands from 950 to 942 cm<sup>-1</sup>. This can be attributed to the coordination of uranyl nitrate complex by TBP resulting in the weakening of U=O bands.

Figure 5 also shows the differential ATR-FTIR spectrum of uranyl nitrate solution in C<sub>4</sub>mimNTf<sub>2</sub>, at various mole ratios of U : NO<sub>3</sub> : TBP : Cl, varied from 1 : 2 : 2 : 0 to 1 : 2 : 2 : 6. The differential spectrum shows the gradual shift of O=U=O asymmetric stretching bands from 942 cm<sup>-1</sup> to 916 cm<sup>-1</sup> when the mole ratio of U : NO<sub>3</sub> : TBP :

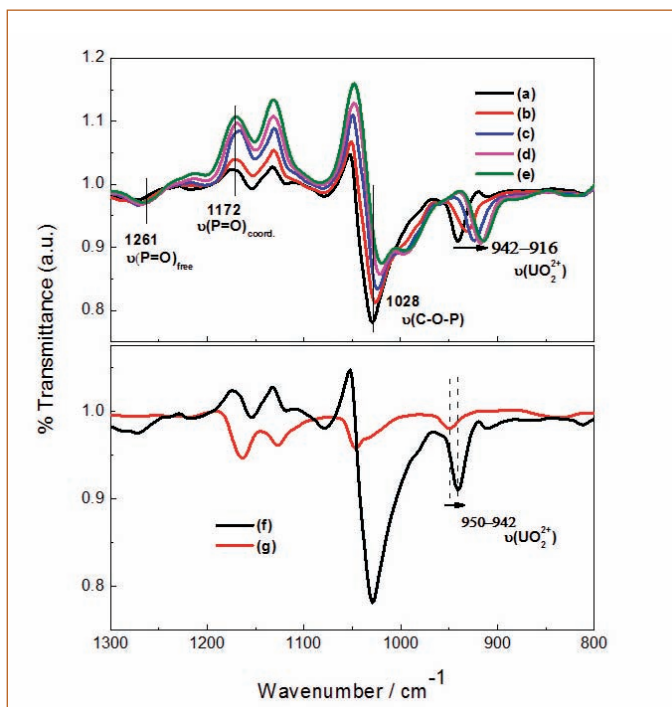


Figure 5: ATR-FTIR spectrum of 80 mM UO<sub>2</sub>(NO<sub>3</sub>)<sub>2</sub> dissolved in C<sub>4</sub>mimNTf<sub>2</sub> containing TBP (160 mM), in the presence and absence of C<sub>4</sub>mimCl. The mole ratio of U : NO<sub>3</sub> : TBP : Cl is 1 : 2 : 2 : 0 in (a), 1 : 2 : 2 : 1 in (b), 1 : 2 : 2 : 2 in (c), 1 : 2 : 2 : 4 in (d), 1 : 2 : 2 : 6 in (e), 1 : 2 : 2 : 0 in (f) and 10 mM UO<sub>2</sub>(NO<sub>3</sub>)<sub>2</sub> dissolved in C<sub>4</sub>mimNTf<sub>2</sub> without TBP (g).

Table 1. Proposed uranyl species existing at various mole ratios of U : NO<sub>3</sub> : TBP : Cl.

Mole ratio of U : NO <sub>3</sub> : TBP : Cl	Dominant uranyl species
1 : 2 : 2 : 0	UO <sub>2</sub> (NO <sub>3</sub> ) <sub>2</sub> (TBP) <sub>2</sub>
1 : 2 : 2 : 1	[UO <sub>2</sub> (NO <sub>3</sub> ) <sub>2</sub> Cl] <sup>-</sup> , UO <sub>2</sub> (NO <sub>3</sub> ) <sub>2</sub> (TBP) <sub>2</sub> <sup>*</sup>
1 : 2 : 2 : 2	[UO <sub>2</sub> (NO <sub>3</sub> )Cl <sub>2</sub> ] <sup>-</sup> , [UO <sub>2</sub> (NO <sub>3</sub> ) <sub>2</sub> Cl <sub>2</sub> ] <sup>2-</sup> <sup>*</sup>
1 : 2 : 2 : 4	[UO <sub>2</sub> (NO <sub>3</sub> )Cl <sub>3</sub> ] <sup>2-</sup> , [UO <sub>2</sub> Cl <sub>4</sub> ] <sup>2-</sup> <sup>*</sup>
1 : 2 : 2 : 6	[UO <sub>2</sub> Cl <sub>4</sub> ] <sup>2-</sup> , [UO <sub>2</sub> (NO <sub>3</sub> )Cl <sub>3</sub> ] <sup>2-</sup> <sup>*</sup>

<sup>\*</sup> indicates that the abundance of that species is quite less as compared to the other co-existing dominant species.

Cl was increased from 1 : 2 : 2 : 0 to 1 : 2 : 2 : 4. Further addition of Cl<sup>-</sup> ions does not shift the position of transmittance bands from 916 cm<sup>-1</sup>. All these observations indicate that uranyl nitrate in TBP/C<sub>4</sub>mimNTf<sub>2</sub> exists in the form of UO<sub>2</sub>(NO<sub>3</sub>)<sub>2</sub>(TBP)<sub>2</sub>; however the addition of Cl<sup>-</sup> ions to the solution gradually substitutes the nitrate ion present in the uranium coordination sphere by Cl<sup>-</sup> ions. When the mole ratio of U : NO<sub>3</sub> : TBP : Cl is 1 : 2 : 2 : 4 or above (i.e., Cl<sup>-</sup> is more) majority of uranyl ion exists in the form of [UO<sub>2</sub>Cl<sub>4</sub>]<sup>2-</sup> in ionic liquid medium. These results are in good agreement with results from visible absorption and Raman spectroscopy of uranyl species discussed above.

#### ATR-FTIR Spectroscopy of P=O Stretching

The ligand TBP exhibits a strong P=O stretching transmittance bands at ~1280 cm<sup>-1</sup>. The differential ATR-FTIR spectrum shows that the transmittance bands at 1172 cm<sup>-1</sup>, which is due to the stretching bands of coordinated P=O groups with uranyl ion. It is interesting to note that the intensity of the differential spectrum at 1172 cm<sup>-1</sup> increases above the value of unity when the mole ratio of U : NO<sub>3</sub> : TBP : Cl increases from 1 : 2 : 2 : 0 to 1 : 2 : 2 : 6. The increase in the transmittance value above unity in the differential spectrum can be taken as an indicative to lowering of the abundance of coordinated P=O groups upon increasing the Cl<sup>-</sup> ion content. This can be possible only when TBP is decomplexed from the uranyl coordination sphere upon Cl<sup>-</sup> addition.

Based on the spectroscopic studies discussed above, the following conclusions can be drawn. Table 1 summarises the dominant uranyl species as a function of Cl<sup>-</sup> ions at various U : NO<sub>3</sub> : TBP : Cl mole ratios. Since Cl<sup>-</sup> is a strong field ligand as compared to the neutral TBP and nitrate ions, the addition of Cl<sup>-</sup> ions gradually displaces the TBP and substitutes the nitrate ions present in the uranyl coordination sphere. Addition of C<sub>4</sub>mimCl changes the nature of uranyl species from UO<sub>2</sub>(NO<sub>3</sub>)<sub>2</sub>(TBP)<sub>2</sub> to [UO<sub>2</sub>Cl<sub>4</sub>]<sup>2-</sup> with the change in mole ratio of U : NO<sub>3</sub> : TBP : Cl from 1 : 2 : 2 : 0 to 1 : 2 : 2 : 6.

G. Murali Krishna  
Materials Chemistry & Metal Fuel Cycle Group

## Conference and Meeting Highlights

### IGCAR - CEA Meeting in Nuclear Technology

#### 14<sup>th</sup> Annual Meeting on LMFBR Safety

October 1-5, 2018

14<sup>th</sup> CEA-IGCAR annual meeting to review ongoing collaborative projects was organized during October 1-5, 2018 through Video Conference. This meeting is the result of cooperation between India and France in the last few decades in the area of application of Nuclear Technology for peaceful purposes. IGCAR and CEA have worked together in the field of liquid metal fast breeder reactor safety through collaborative projects. IGCAR team was led by Dr. Arun Kumar Bhaduri, Distinguished Scientist and Director IGCAR and the CEA team was led by Dr. Christian Latge, Technical Coordinator CEA. Thirty three IGCAR experts and thirty one CEA experts participated in the annual meeting. Meetings were divided into one plenary session and nine technical sessions for discussion on topics namely NDT, Instrumentation, Sodium Fire, Reactor Safety, Fuel Safety, Severe Accident etc. In the plenary session, status of PFBR, FBTR and ongoing R&D for FBR were presented by IGCAR whereas CEA presented status of Advanced Sodium Technological Reactor for Industrial Demonstration (ASTRID). Status of ongoing Implementing Agreement (IA) and new topics for potential collaboration were discussed during the meeting. The annual meeting through video conference was a new experiment and was fruitful & successful.

#### Technical Annual Meeting for JHR Collaboration

November 13, 2018



Delegates of IGCAR-CEA Technical meeting held at the Centre

A Technical Annual Meeting of IGCAR- CEA for Jules Horowitz Reactor (JHR) Collaboration was held on November 13, 2018 at IGCAR, Kalpakkam. IGCAR team consisting of sixteen experts was led by Dr. P. Selvaraj, Director-FRTG and CEA team consisting of five experts was led by Dr. Gilles Bignan, JHR User Facility Interface Manager at CEA, France. Dr. P. V. Varde, Associate Director, Reactor Group represented BARC. In the opening remarks, Dr. Gilles Bignan briefed about the current status of JHR Project in France and Dr. P. Selvaraj enumerated experiments carried out in the Research Facility for Irradiation studies in Sodium at High temperature (RISHI) loop in IGCAR. Technical presentations on the Heat transfer system, Design and Development of Specimen Chamber & Sodium Level Probe, Testing and handling of RISHI loop at FBTR were made by IGCAR experts. The French team visited and witnessed an experiment conducted in RISHI loop at FRTG. The technical annual meeting was fruitful & successful.

*Reported by  
Dr. B. K. Nashine, Coordinator, IGCAR-CEA*

## Conference and Meeting Highlights

### 26<sup>th</sup> Prof. Brahm Prakash Memorial Materials Quiz Grand Finale (BPMMQ 2018)

October 5 -6, 2018



Dr. Arun Kumar Bhaduri, Distinguished Scientist and Director, IGCAR addressing the participants

The 26<sup>th</sup> Prof. Brahm Prakash Memorial Materials Quiz Grand Finale was conducted in a grand manner at Indira Gandhi Centre for Atomic Research during October 5-6, 2018. This year saw the participation from 37 teams representing 22 chapters of Indian Institute of Metals (IIM) across the country. The students were from classes XI and XII and were accompanied by teachers for this event.

On October 05, 2018, a visit to nuclear facilities in Kalpakkam, popularly known as the 'Metal Camp' programme was arranged. The student participants and teachers assembled in Sarabhai Auditorium at IGCAR Campus and Dr. R. Divakar, Chairman, IIM Kalpakkam Chapter welcomed them. Following this, Dr. G. Amarendra, Director, MSG & MMG and Chairman, BPMMQ Organising Committee, addressed the students and briefed them about the visits to the various facilities during the day. Dr. Shaju K. Albert, Associate Director, MEG, MMG recollected his association with the quiz in earlier years and described its rapid growth of popularity over the years. After watching a video on the science of nuclear energy, the students and teachers visited FBTR, MAPS and BHAVINI.

On October 06, 2018 the students assembled at the Training School seminar hall for the Prof. Brahm Prakash Memorial Materials Quiz event. Dr. V. S. Srinivasan welcomed the participants and briefed them the details of technical programme. This was followed by computerised draw of lots by Dr. G. Amarendra, Director, MSG & MMG. The preliminary rounds were held in six parallel sessions and the winner and runner of each session were chosen for semi finals. The semi finalists were Kolkata A & B, Chennai B, Coimbatore B, Trichy A, Kalpakkam A, Raigarh A & B, Ranchi A, Kanpur A, Mumbai and Bhopal. Six teams from the semi finals, namely, Trichy A, Chennai B, Raigarh A, Ranchi A, Mumbai and Bhopal qualified for the finals.

The Prof. Brahm Prakash Memorial Lecture 2018 was delivered by Dr. A. K. Bhaduri, Distinguished Scientist and Director, IGCAR on the topic "Improved Materials & Fabrication Technologies for the Indian Fast Breeder Reactor Programme". He emphasized the need to engineer structural materials to withstand the fast reactor environment. He also described various innovative techniques for fabricating various components of the fast breeder reactor and disclosed how intricate fast reactor components fabricated in India have drawn appreciation in the international arena.

The BPMMQ Grand Finale was conducted by Dr. Sumanth C. Raman, a renowned doctor with TCS, Chennai and a popular quiz master. In a closely contested final, IIM Trichy Team comprising of Shri Jeya Amirthan and Shri S. Natarajan from Sri Jayendra Saraswathi Swamigal Silver Jubilee MHSS won the first prize and IIM Chennai Team comprising of Shri G. Karthik Balaji and Shri Manav Tathacharva from Padma Seshadri Bala Bhavan Senior Secondary School, K. K. Nagar, Chennai won the second place.

*Reported by  
Dr. V. D. Vijayanand, Convener, BPMMQ-2018*

## Conference and Meeting Highlights

### National Conference URJAVARAN – 2018

November 15-16, 2018



Dr. G. Amarendra, Director, MSG & MMG, Shri C. Chandran, Convener, Shri P. V. Kumar, Former Project Director, FRFCF, Shri Jenson Sebastian, RD, ISHRAE and Shri Anil Kumar Sahoo, Organising Secretary during the inaugural function

Air-Conditioning & Ventilation System Division (AC&VSD), IGCAR in association with Indian Society of Heating Refrigerating & Air-conditioning Engineers (ISHRAE) - Kalpakkam Sub-Chapter organized the 3<sup>rd</sup> National Conference URJAVARAN – 2018 at Sarabhai Auditorium, IGCAR during November 15-16, 2018. About two hundred and seventy-five delegates from academic institutions, industries, R&D organizations and leading consultants attended the conference.

In the inaugural function, Shri C. Chandran, Convener, URJAVARAN – 2018 & Head, AC&VSD, ESG delivered the welcome address & briefed about the conference and the impact on ENVIRONMENT and CLIMATE due to increase in air-conditioning load. The inaugural function was presided over by Dr. G. Amarendra, Director, MSG & MMG. In his presidential address, Dr. G. Amarendra, emphasized the importance of energy conservation, energy efficiency and expressed his concern about degradation of environment. Shri P. V. Kumar, former Project Director, FRFCF delivered the keynote address on the topic "Design aspects of Ventilation for Nuclear Facilities" and highlighted the various design intricacies of ventilation system for reprocessing plants and nuclear establishments and shared his experience of active ventilation systems for nuclear facilities. The Conference souvenir was released by Dr. G. Amarendra & Shri P. V. Kumar. Shri Anil Kumar Sahoo, Organizing Secretary, URJAVARAN - 2018 proposed the vote of thanks. Dr. G. Amarendra Director, MSG & MMG inaugurated the exhibition stalls of exhibitors & industrial partners. Various industries of high repute, in the field of Heating Ventilation & Air Conditioning (HVAC) system and component design showcased their products at the venue of conference and shared the specific features of the products.

The conference discussed latest trends, ongoing research, and innovative implementation and energy conservation measures in HVAC systems. It included invited talks by eminent speakers from academic institutions, industries, R&D organizations and leading consultants in the areas of green building, solar air-conditioning, CO<sub>2</sub> refrigeration, air-conditioning and ventilation of hospitals. A representative from Energy Efficiency Services Limited delivered a special talk on implementation of energy efficiency programs by Government of India. Eighteen contributed papers from DAE units (IGCAR, BARC & MAPS) and academic institutions on green buildings, energy conservation, air-conditioning & ventilation of nuclear facilities were presented during the conference. Product presentations from reputed industries were also part of the conference. The conference facilitated good interactions among delegates and experts in the area of HVAC.

During the valedictory function, Shri Faizan Ullah Khan, Convener, Technical Committee, URJAVARAN-2018 summed up the two day conference. Dr. B. Venkatraman, Director, HSEG & RMPAG delivered the valedictory address, highlighting the importance of innovations in technologies to conserve energy. He also emphasized the requirement of utilizing the expertise of invited speakers in the design of hospital ventilation for the department. Shri C. Chandran proposed the vote of thanks.

*Reported by  
Shri C. Chandran, Convener, URJAVARAN-2018*

## Conference and Meeting Highlights



### Indo-UK Civil Nuclear Collaboration Review Meeting

December 3-5, 2018

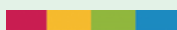


Delegates of Indo-UK workshop meet, with Dr. Arun Kumar Bhaduri, Distinguished Scientist and Director, IGCAR and other senior colleagues of the Centre

Indo-UK Civil Nuclear Collaboration Review Meeting was organized during December, 3-5, 2018. IGCAR, on behalf of DAE, was the nodal agency to host the event and it was held at Welcome hotel Kences Palm Beach, Mamallapuram. Seventeen delegates from UK, twenty six from IGCAR and twenty five from BARC attended the meeting. On 3<sup>rd</sup> December 2018, the team from UK visited IGCAR and Dr. Arun Kumar Bhaduri, Distinguished Scientist and Director IGCAR made a presentation about the ongoing activities of IGCAR to the participants. Subsequently the delegation from U. K. visited selected laboratories at IGCAR. The meeting on December 4-5, 2018 was jointly inaugurated by Shri Arun Srivastava, Head of Institutional Collaborations and Programs, DAE and Professor Robin Grimes, Chief Scientific Advisor for Ministry of Defence on nuclear science and technology matters, U. K. Presentations on Phase 1 to Phase 4 of ongoing and completed collaborative projects were made by respective project coordinators. Presentations on potential new projects in the field of Waste Management, new Nuclear Systems including Plant Design, Materials, Advanced Manufacturing, Nuclear Safety and Security, Thermal Hydraulics and Environmental Remediation etc. were made by experts from both the countries. During the discussion, possible collaborative projects were listed to facilitate evolution of final list of agreed collaborative projects in the next meeting.

*Reported by  
Dr. B. K. Nashine, FRTG*

## Conference and Meeting Highlights



### Report on Radiation Awareness Program at Kalpakkam

December 8, 2018



Ms. M. Manohari, HSEG, Dr. Padma S. Kumar, Treasurer, IWSA-K, Dr. R. Baskaran, AD, RESG, HSEG, IGCAR, Dr. Anita Toppo, Secretary, IWSA-K during inaugural session

A one day program on nuclear energy and radiation safety awareness was organised by HSEG, IGCAR in association with Indian Women Science Association (IWSA), Kalpakkam Chapter on December 8, 2018 at Multipurpose Hall, Kalpakkam. 175 enthusiastic women participants from Kalpakkam Township attended the program which was conducted both in English and Tamil.

The Morning session had audience who have opted for English language presentation. Dr. Padma S. Kumar, welcomed the gathering. Dr. Anita Toppo, presented the activity report of IWSA-K, highlighting the recent programs organised by the professional body. Dr. R. Baskaran, AD, RESG, HSEG, IGCAR was the chief guest for the program and he addressed the participants about the need for nuclear energy, details of nuclear facilities at Kalpakkam, aspects of radiation protection and the applications of radiation. He also inaugurated an exhibition organised by TC&PAS, MAPS and ESL.

The Tamil session was held in the afternoon. Shri. R. Mathiyarasu, Head, RBDS, RESG, IGCAR, delivered the lecture in Tamil giving many examples from day to day activities. Both the English and Tamil lectures were followed by an interactive session, conducted by the senior scientists from HSEG, IGCAR. This session which had many games interspersed with questions from the audience was highly appreciated. The visit to exhibition enabled further interaction. The program ended with a vote of thanks by Dr. Gurpeet Kaur, IWSA (K). This event succeeded in motivating women residents to raise questions and get better clarity on aspects relating to Nuclear energy through interaction with scientists from IGCAR.

*Reported by  
Dr. S. Chandrasekaran, HSEG*

## Conference and Meeting Highlights

### Second Quadrennial International Conference on Structural Integrity (ICONS2018)

December 14-17, 2018 @ IITM Chennai



Prof. Raghu Prakash, Dr. B. Purna Chandra Rao, Dr. G. Amarendra, Dr. Arun Kumar Bhaduri, Shri Nandkumar Athawale, Prof. Koshy Varghese, Dr. G. Sasikala, Shri R. Suresh Kumar

Second quadrennial International Conference on Structural Integrity (ICONS2018) was jointly organized by Indira Gandhi Centre for Atomic Research (IGCAR), Kalpakkam and Society for Failure Analysis (SFA), Chennai Chapter together with Indian Institute of Technology Madras, Chennai, Indian Structural Integrity Society (InSIS), Bengaluru and Indian Institute of Science, Bengaluru during December 14-17, 2018 at IITM Chennai. ICONS2018 was also endorsed by Italian Group of Fracture (IGF).

In the inaugural function, Prof. Raghu Prakash, Chairman, ICONS2018, delivered the welcome address & Dr. G. Sasikala, Chairperson, ICONS2018 briefed about the conference. The function was presided over by Dr. G. Amarendra, Chairman National Advisory Committee, ICONS2018 and the conference was inaugurated by Dr. Arun Kumar Bhaduri, Distinguished Scientist and Director, IGCAR, in the presence of Shri Nandkumar Athawale, Vice President, Design & Engineering Centre, Defence & Aerospace, L&T Ltd. In the inaugural address, Dr. Arun Kumar Bhaduri, Distinguished Scientist and Director, IGCAR gave recommendations to expand the scope of ICONS based on the recent incidents and trends. Shri Nandkumar Athawale, Guest of honour, highlighted the challenges experienced in the area of structural integrity in the defence sector. To commemorate the occasion, an abstract-cum-souvenir was released. Prof. Koshy Varghese, Dean-Administration, IIT Madras and Dr. B.P.C. Rao, President SFA, addressed the gathering and Shri. R. Suresh Kumar, Convener ICONS2018 proposed the vote of thanks.

ICONS2018 brought together leading Engineers & Scientists from nuclear, aerospace, defence, chemical & oil industries, academic researchers and research scholars from IISc, IITs, NITs and other academic institutions to exchange their experience and research results in various aspects of structural integrity. About 225 participants attended the conference and made a wide range of presentations. These presentations were made in parallel sessions such as structural integrity and life extension, fatigue and fracture mechanics, failure analysis, structural health and condition monitoring, advanced structural materials, creep and creep-fatigue interaction, computational and numerical fracture mechanics, design and stress analysis, damage mechanics, reliability and regulatory aspects. There were 7 plenary, 23 invited and 132 contributory presentations. Among the 132 full-length manuscripts that were accepted after peer review, 20 were selected for publication in the IGF journal (*Frattura ed Integrità Strutturale*), 75 have been recommended for publication in the Springer Nature as a special volume in Springer Lecture Notes in Mechanical Engineering and the remaining will be published as ICONS2018 conference proceeding.

Prizes were awarded to 3 best oral presentations, 3 best poster presentations in the general category and 4 best poster presentation in the students category. These were distributed during the valedictory function by Dr. Elaya Perumal, Senior Corrosion and Metallurgical Consultant.

*Reported by  
Shri R. Suresh Kumar, Convener, ICONS2018*

## HBNI-IGCAR Corner

## Research Contribution Awards

## Raman spectroscopic and computational studies on diisopropylammonium perchlorate

Ms. Shradhanjali Sahoo, Dr. T. R. Ravindran, Dr. Sharat Chandra

7<sup>th</sup> International Conference on Perspectives in Vibrational Spectroscopy (ICOPVS-2018) held at BARC, Mumbai, November 25-28, 2018.

## Best Poster Award

Dr. K. Srinivasan, MSG, IGCAR won the Best Thesis Award at 63<sup>rd</sup> DAE Solid State Physics Symposium held at Guru Jambheshwar University of Science & Technology, Haryana, December 18-22, 2018

Dr. D. Sanjay Kumar has been selected by Indian Association of Nuclear Chemists and Allied Scientists (IANCAS) for Prof. H.J. Arnika Best Thesis Award for the year 2018

## Ph.D Thesis Defense

Name	Title	Date	Discipline
Mr. K. C. Pitchaiah	Solubility studies on ligands in supercritical carbon dioxide medium and their application to extraction of actinides	26.10.2018	Chemical Sciences
Mr. J. Abuthahir	Studies of magnetic field induced domain wall dynamics in polycrystalline iron and iron based alloys using magnetic force microscopy	17.10.2018	Physical Sciences
Ms. Gurpreet Kaur	Effect of correlation and disorder on the properties of uranium based compounds: first principles calculations	26-10-2018	Physical Sciences
Mr. Nilakantha Meher	Dynamics and control of photon transport in coupled cavities	19.11.2018	Physical Sciences
Mr. Kishore Kumar Madapu	Near-field optical properties of InN nanostructures	28.11.2018	Physical Sciences
Mr. K. A. Irshad	Studies on crystal structure of functional rare earth sesquioxides at high pressures	19.12.2018	Physical Sciences
Ms. Madhusmita Sahoo	Structural and wetting studies of visible light active TiO <sub>2</sub> thin films	20.12.2018	Physical Sciences
Mr. Nair Radhikesh Raveendran	Magneto-transport and magnetization studies on the electron doped cuprate superconductor Nd <sub>1.85</sub> Ce <sub>0.15</sub> CuO <sub>4-δ</sub>	21.12.2018	Physical Sciences
Ms. G. Sumathi	Secure and Reliable VLSI Designs	26.11.2018	Engineering Sciences

## DAE Awards



Department of Atomic Energy has instituted annual awards for excellence in Science, Engineering and Technology in order to identify best performers in the area of Research, Technology Development and Engineering in the constituent units (other than Public Sector Undertakings and Aided Institutions). The Young Applied Scientist, Young Engineer, Young Technologist, Homi Bhabha Science and Technology Award and Scientific and Technical Excellence Award fall under this category. Group Achievement awards for recognition of major achievements by groups have also been instituted. Life-time Achievement Award is awarded to one who has made significant impact on the DAE's programmes. They are the icons for young scientists and engineers to emulate. The awards consist of a memento, citation and cash prize.

### The recipients of the Awards from IGCAR for the year 2017 were:

<b>Young Scientist Award</b>	: Dr. Amit Kumar, HSEG
<b>Young Applied Scientist/Technologist Award</b>	: Shri J Christopher, MMG Shri Joel Jose, FRTG
<b>Scientific and Technical Excellence Award</b>	: Dr. A. Nagesha, MMG Dr. Rajesh Ganesan, MC&MFCG Shri V. Vinod, FRTG
<b>Young Engineer Award</b>	: Shri Kulbir Singh, RDG Shri S. Sathiskumar, FRTG Shri Muhammad Sabih, FRTG
<b>Meritorious Service Award</b>	: Ms. Hema Ravichandran, RFG Shri P. Jayabalan, CC
<b>Meritorious Technical Support Award</b>	: Shri M. Muthukumaraswamy, RFG Shri R. Viswanathan, RFG Ms. K. Shyamala Devi, HSEG

### Group Achievement Awards:

Design, Development, Integration and Testing of a Indigenous Plutonium Continuous Air Monitor (PuCAM)

Ms. L. Srivani, EIG, Group Leader

Shri N. Anil, Shri Alok Kumar Gupta, Shri K. Elangovan, Shri K. Praveen and Shri M. Thangadurai from EIG; Shri J. Abilash, Shri P. Balakrishnan, Shri N. Chockalingam, Shri D. Dileep, Shri M. Krishnamoorthy, Shri C. Muthusamy, Shri A. Padmanabhan, Shri B. Ramalingam, Shri S. Ramesh, Shri P. Shanmugam, Shri C. Siva and Shri E. Venkatesan from ESG; Shri K. C. Ajoy, and Shri A. Dhanasekaran from HSEG; Dr. G. Raghavan from MSG; Shri Amit Kumar Dash, Shri D. Anandaraj, Shri Avik Kumar Saha, Shri R. Raghunath, Shri P. Vijayasekaran, Shri Geo Mathews, Shri P. Varadharajan, Shri S. Somasundaram and Shri Saju George from RpG; Shri C. R. Venkatasubramani, RRF (Retired); Dr. V. Anita Topkar, Ms. Aggarwal Bharti, Shri H. H. Vaity, Shri C. P. Kulkarni, Shri S. Chakraborty, Shri M. M. Kuswarkar, Shri Mahesh Punna, Shri M. U. Pawar, Shri L. V. Murali Krishna, Ms. S. Padmini and Shri S. K. Patil from E&IG, BARC.

### Identification and Replacement of failed Steam Generator for the first time in FBTR

**Shri K. G. Subramanian, RFG, Group Leader**

Shri K. V. Suresh Kumar, Shri A. Babu, Shri S. Sridhar, Shri P. V. Anilkumar, Shri D. Chandrasekaran, Shri M. Babu, Shri E. Ramesh, Shri M. Elango, Shri K. Ramachandran, Ms. Liji Jacob, Shri P. Ragothkumar, Shri G. Shanmugam, Shri N. Manimaran, Shri V. Alagudurai, Shri A. Suriyanarayanan, Shri D. Vignesh Babu, Shri R. Sekar, Shri N. Sampathkumar, Shri S. Kanagaraju, Shri P. Balamurali, Shri A. Ramamoorthy, Shri N. Ranjithkumar, Shri G. Kannan, Shri N. Kathiresan, Shri R. Desingu, Shri M. Karthikeyan, Shri J. Manikandan, Shri R. Vedhamanickam, Shri K. Kamaludeen, Shri R. Gopal, Shri M. Muthukumarasamy, Shri A. Nagalingam, Shri Syed Saleem, Shri C. Kannan, Shri M. Chitrarasu, Shri V. Velu, Shri V. Govindaraj, Shri M. Jayasankar, Shri N. Manivel, Shri G. Narayanassamy, Shri M. Sounder, Shri D. Jaisrinivasan, Shri A. Udaya Sankar, Shri N. Basavaiah, Ms. N. K Lakshmi, Ms. P. Thyyal Nayaghi, Ms. R. Vasanthi, Ms. S. Manjula, Shri Raghav Sharma, Shri A. Lakshmanan, Shri S. Sathish Kumar, Shri K. Perumal, Shri D. Gautham, Shri Sachin Kale, Shri Ashok D Hanimana, Shri M. S Koteeswaran, Shri K. Prakash, Shri R. Vijayanand, Shri Vijayavarman, Shri S. Sathish, Shri D. Samayaraj, Shri S. Haridas, Shri Challa Ravikumar, Shri Shyam Ravikumar, Shri Manoj Kumar Agarwal, Shri Balamurugan, Shri P. Munuswamy, Shri Jayamoorthi, Shri M. Uthaman, Shri A. Thandavamurthy, Shri R. Balasubramaniam, Shri K. Ganapathy Subramanian, Shri S. Sathish kumar, Shri A. M. Kannan, Shri B. Mohanarangan, Ashish D Jain Shri J. Sasikumar, Shri M. Thangamani, Shri D. Vinoth, Shri S. Joy, Shri K. Gopal, Ms. S. Anthoniammal, Shri D. Ezhilan, Shri V. Sreenivasan from **RFG**; Shri B. Anandapadmanaban, Shri N. Raghu, Shri G. Ramesh, Shri Saju T. Abraham, Ms. Alka Kumari, Shri P. Azhagesan, Ms. D. Chitra, Shri P. Narayana Rao, Shri Henson Raj, Shri D. Kuppusamy, Shri R. Rajesh and Shri G. Vijaya Raghavan from **HSEG**; Dr. B. P. C. Rao, Dr. A. Joseph, Dr. G. K. Sharma, Ms. T. Nivedha from **MMG**; Shri E. Premkumar from **RM&PAG**

### Design, Manufacturing, Erection Commissioning and Operation of Sodium Facility for Component Testing (SFCT)

**Dr. C. Meikandamurthy FRTG, Group Leader**

Shri S. Chandramouli, Shri R. Punniyamoorthy, Shri A. Ashokkumar, Shri S. Ravishankar, Shri D. Muralidhar, Shri Parmanand Kumar, Shri A. Thirunavukkarasu, Shri C. Rajappan, Shri N. Sreenivas, Shri K. Arumugam, Shri P. R. Ashokkumar, Shri L. Eagambaram, Shri J. Prabhakaran, Shri M. Karthikeyan, Shri Shaik Rafee, Shri K. Ganesh, Shri Ashish Tiwari, Shri L. Mohanasundaram, Shri L. Muthu, Shri Vijay Tirkey, Shri G. Vijayakumar, Shri R. Rajendraprasad, Shri Gautam Anand, Shri R. Iyappan, Shri R. Parandaman, Shri S. Kannan, Shri P. Lakshmayya, Shri P. Pothi, Ms. M. Chandra, Shri P. Rajasundaram, Ms. P. Anitha, Shri M. V. Subramanya Deepak, Shri T. V. Maran, Shri K. Mohanraj, Shri A. Anthuvan Clement, Shri K. Ramesh, Shri V. Ramakrishnan, Shri M. Anandaraj, Shri D. Laxman, Shri R. Rajendran, Shri S. Shanmugam, Shri H. Rafiq Basha, Shri M. Kathiravan, Shri K.A. Bijoy, Shri A. Selvakumaran, Dr. B. Babu, Shri T. Chandran, Ms. Shanthi Rajendran, Shri Rakesh Kumar Mourya, Shri S. Ignatius Sundar Raj, Shri S. C. S. P. Kumar Krovvidi, Shri A. Kolanjiappan, Shri R. Ramalingam, Shri J. Saravanan, Shri Anant Kumar, Shri V. Vinod, Shri M.G. Hemanath, Shri S. Sathishkumar, Shri Muhammad Sabih, Shri S. Balakrishnan, Shri S. Alexander Xavier, Shri N. Venkatesan, Shri P. Chenthilvelmurugan, Shri N. Mohan, Shri J. Prem, Shri V. Gunasekaran, Shri B.K. Nashine, Ms. S. Saravana Priya, Ms. Kamalambigai from **FRTG**; Shri N. Raghu, Shri G. Ramesh, Shri M. V. Kuppusamy, Shri C.B. Rajeev, Ms. D. Chitra, Shri Shri Krishna Tripathi, Shri Navtesh Bajpai, Shri D. Hensonraj, Shri P. Narayana Rao, Shri K. Murugan from **HSEG**; Shri N. Suresh, Shri H. I. Abdul Gani, Ms. R. Thilakavathy, Ms. K. Subhashini from **ESG**.

## Awards and Honours

Dr. Shaju K. Albert, MEG, MMG has been inducted as Associate Editor of the Welding in the World, an Official Journal of International Institute of Welding

Dr. Anita Toppo, Corrosion Science & Technology Division (CSTD), MMG received "Corrosion Awareness Award – 2018" for Distinction in Corrosion Science & Technology in Research & Education from NACE International Gateway India on October 02, 2018

Dr. R. Divakar, PIED, MMG has been conferred the Metallurgist of the year Award in Metal Science category for the year 2018 from the Ministry of Steel, Government of India

Dr. B. K. Sreedhar, Dr. Shaju K. Albert and Dr. A. B. Pandit have been awarded Dr. S. Parthasarthy Memorial Award for the year 2017 by Ultrasonics Society of India for the paper titled "Computation of Erosion Potential of Cavitation Bubbles in Ultrasonic Pressure Field" published in Journal of pure and applied ultrasonics. 39 (2017) 60-69. The award was presented on November 12, 2018 by Ultrasonics Society of India

Detection of Hydrogen Assisted Cracking Susceptibility in Modified 9Cr-1Mo Steel Welds by Acoustic Emission Technique

Dr. Gopa Chakraborty, Shri O. Venkata Ramana, Shri T. K. Haneef, Dr. Shaju K. Albert, Dr. Babu Rao Jinugu, Dr. C. K. Mukhopadhyay and Dr. B. P. C. Rao

Presented at the International Congress 2017 (IC-2017) held at the Chennai Trade Centre, Chennai during December 7-9, 2017, has been adjudged the winner of Sharp Tools Award - 2018 by the Indian Institute of Welding. The award was presented on December 13, 2018

Dr. C.K. Mukhopadhyay, NDED, MMG received ISNT National NDT Award in R & D during National Seminar on NDE (NDE-2018) at Mumbai, December 19-21, 2018

National QC Meet (NCQC -2018) at IIIT, Gwalior, December 19-24, 2018

Shri A. Mainvannan, Ms. Dinu Shaji, Shri G. Saravanan, Shri S. Maharajan, Ms. R. Jayashree and Shri M. Santosh FERMI team of MFFD, MC&MFCG received "Par Excellence" award for the case study presentation on "Minimizing the Downtime in Sodium Bonding Furnace"

Shri R. R. Shridharan, Shri D. Alagar, Shri E. Radha, Shri D. Seenivasan, Shri M. S. Murugappa and Shri V. Nandakumar EXCEL team of PPED, MC&MFCG received "Excellence" award for the case study presentation on "Reduction of Interruption Time in Nitrogen Generation System (NGS) Furnace"

Shri K. Murugan, Shri P. Azhagesan, Shri S.P. Manivannan, Shri D. Suresh, Shri P. Ettiyappan and Shri P. Chentil Kumar, QAD, HSEG, 5S Team, received "Par Excellence Award" for the Case Study Presentation titled "Guide for Ultrasonic Examination of Nozzle Welds"

## Best paper/Poster Awards

Interdisciplinary Symposium on Material Science 2018 (ISMC 2018) held in BARC, Mumbai, December 4-8, 2018

Development of Ytria Coating on the Inner Surface of Quartz Tube for Metal Alloy Casting

Shri M. Rahman Mollah, Shri A. V. Vinod and Dr. Soumen Das

Laser Ablated Thin Films of PbS for Ammonia Sensing under Inert Ambient

Ms. T. V. Beatrice Veena, Dr. E. Prabhu and Dr. K. I. Gnanasekar

Preliminary Studies on the Oxidation of Rare Earth (La, Gd) Chlorides in LiCl-KCl

Shri Pabitra Ghosh, Dr. Manish Chandra, Shri P. Venkatesh, Dr. K. S. Mohandas and Dr. B. Prabhakara Reddy

Best Poster Awards

CORCON 2018, held during September 30 - October 03, 2018 in Jaipur

A Novel Chitosan/Ag/Go Composite Coating with Enhanced Antibacterial Activity and Improved Corrosion Resistance

Ms. Geetisubhra Jena, Dr. B. Anandkumar, Dr. S. C Vanithakumari, Dr. Rani P. George, Dr. John Philip and Dr. G. Amarendra

High Performance Green Concrete with Improved Biodeterioration Resistance against Fungus Fusarium

Shri Manu Harilal, Ms. Sudha Uthaman, Dr. B. Anandkumar, Dr. Rani P. George, Dr. John Philip and Dr. G. Amarendra

Best Poster Awards

Self - healing Plasma Spray Coatings on Graphite for High Temperature Applications

Ms. B. Madhura, Shri E. Vetrivendan, Dr. Ch. Jagadeeshwara Rao and Dr. S. Ningshen

Best Paper Award

## Biodiversity Basket - Avian Fauna



Pied Kingfisher



Pied Kingfisher has a prominent black and white streaked crest. It has a stout and pointed dagger like bill. Females are similar to males. A black necklace like gorget broken in the middle is male.

**Editorial Committee Members:** Dr. T. S. Lakshmi Narasimhan, Dr. N. V. Chandra Shekar, Dr. C. K. Mukhopadhyay, Dr. Vidya Sundararajan, Shri A. Suriyanarayanan, Dr. C. V. S. Brahmananda Rao, Dr. V. Subramanian, Ms. R. Preetha, Shri J. Kodandaraman, Shri G. Venkat Kishore, Shri S. Kishore, Dr. N. Desigan, Shri M. Rajendra Kumar, Shri V. Rajendran, Ms. S. Rajeswari, Shri K. Ganesan, Shri K. Varathan and Shri G. Pentaiah